Representing key phytoplankton functional groups in ocean carbon cycle models: Coccolithophorids

M. Débora Iglesias-Rodríguez,[1,2] Christopher W. Brown,[3] Scott C. Doney,[4] Joan Kleypas,[4] Dorota Kolber,[1] Zbigniew Kolber,[1] Paul K. Hayes,[5] and Paul G. Falkowski[1,6]

Received 26 June 2001; revised 8 January 2002; accepted 16 July 2002; published 26 November 2002.

[1] Carbonates are the largest reservoirs of carbon on Earth. From mid-Mesozoic time, the biologically catalyzed precipitation of calcium carbonates by pelagic phytoplankton has been primarily due to the production of calcite by coccolithophorids. In this paper we address the physical and chemical processes that select for coccolithophorid blooms detected in Sea-viewing Wide Field-of-view Sensor (SeaWiFS) ocean color imagery. Our primary goal is to develop both diagnostic and prognostic models that represent the spatial and temporal dynamics of coccolithophorid blooms in order to improve our knowledge of the role of these organisms in mediating fluxes of carbon between the ocean, the atmosphere, and the lithosphere. On the basis of monthly composite images of classified coccolithophorid blooms and global climatological maps of physical variables and nutrient fields, we developed a probability density function that accounts for the physical chemical variables that predict the spatiotemporal distribution of coccolithophorids in the world oceans. Our analysis revealed that areas with sea surface temperatures (SST) between 3° and 15°C, a critical irradiance between 25 and 150 μmol quanta m^{-2} s^{-1}, and decreasing nitrate concentrations ($\Delta N/\Delta t < 0$) are selective for upper ocean large-scale coccolithophorid blooms. While these conditions favor both Northern and Southern Hemisphere blooms of the most abundant coccolithophorid in the modern oceans, *Emiliania huxleyi*, the Northern and Southern Hemisphere populations of this organism are genetically distinct. Applying amplified fragment length polymorphism as a marker of genetic diversity, we identified two major taxonomic clades of *E. huxleyi*; one is associated with the Northern Hemisphere blooms, while the other is found in the Southern Hemisphere. We suggest a rule of ''universal distribution and local selection'': that is, coccolithophorids can be considered cosmopolitan taxa, but their genetic plasticity provides physiological accommodation to local environmental selection pressure. Sea surface temperature, critical irradiance, and $\Delta N/\Delta t$ were predicted for the years 2060–2070 using the NCAR Community Climate System Model to generate future monthly probability distributions of coccolithophorids based upon the relationships observed between the environmental variables and coccolithophorid blooms in modern oceans. Our projected probability distribution analysis suggests that in the North Atlantic, the largest habitat for coccolithophorids on Earth, the areal extent of blooms will decrease by up to 50% by the middle of this century. We discuss how the magnitude of carbon fluxes may be affected by the evolutionary success of coccolithophorids in future climate scenarios. *INDEX TERMS:* 1615 Global Change: Biogeochemical processes (4805); 4594 Oceanography: Physical: Instruments and techniques; 4842 Oceanography: Biological and Chemical: Modeling; 4855 Oceanography: Biological and Chemical: Plankton

Citation: Iglesias-Rodríguez, M. D., C. W. Brown, S. C. Doney, J. Kleypas, D. Kolber, Z. Kolber, P. K. Hayes, and P. G. Falkowski, Representing key phytoplankton functional groups in ocean carbon cycle models: Coccolithophorids, *Global Biogeochem. Cycles*, *16*(4), 1100, doi:10.1029/2001GB001454, 2002.

[1]Environmental Biophysics and Molecular Ecology Program, Institute of Marine and Coastal Sciences, Rutgers University, New Brunswick, New Jersey, USA.

[2]Also at School of Biological Sciences, University of Bristol, Bristol, England, UK.

[3]Office of Research and Applications, National Oceanographic and Atmospheric Administration, Camp Springs, Maryland, USA.

[4]National Center for Atmospheric Research, Climate and Global Dynamics, Boulder, Colorado, USA.

[5]School of Biological Sciences, University of Bristol, Bristol, England.

[6]Also at Department of Geology and Institute of Marine and Coastal Sciences, Rutgers University, New Brunswick, New Jersey, USA.

0886-6236/02/2001GB001454$12.00

1. Introduction

[2] Phytoplankton comprise at least eight phylogenetic divisions or phyla, represented by approximately 20,000 extant species [*Falkowski and Raven*, 1997]. In the ocean, these organisms are central to biogeochemical and ecological "services"; that is, they function to link metabolic sequences and properties to form a continuous, self-perpetuating network of elemental fluxes. The biologically mediated fluxes of elements between the upper ocean and the ocean interior are critically dependent upon key groups of phytoplankton. For example, autotrophic carbon fixation converts gaseous CO_2 to a wide variety of organic carbon molecules, virtually all of which are solid or dissolved solids at physiological temperatures ("Fixation" is a term that means to make nonvolatile, as in conversion of a gas to another phase state). Respiration accomplishes the reverse. Nitrogen fixation converts gaseous N_2 to ammonium and thence to organic molecules, while denitrification accomplishes the reverse. Calcification converts dissolved inorganic carbon and Ca to solid-phase calcite and aragonite, whereas silicification converts soluble silicic acid to solid hydrated amorphous opal. Each of these biologically catalyzed processes is dependent upon specific metabolic sequences (i.e., gene families encoding suites of enzymes) that evolved over hundreds of millions of years of Earth's history, and have, over corresponding periods, led to the massive accumulation of calcite, opal, and organic matter in the lithosphere. Presumably because of parallel evolution as well as lateral gene transfer, these metabolic sequences have frequently coevolved in several groups of organisms that, more often than not, are not otherwise closely related from a phylogenetic standpoint [*Falkowski and Raven*, 1997]. On the basis of their biogeochemical metabolism, these homologous sets of organisms can be clustered into "functional groups" or "biogeochemical guilds"; i.e., organisms that are related through common biogeochemical processes rather than phylogenetic affiliation. Here we focus on elucidating the basic physical and chemical processes that select for surface calcifying, bloom-forming phytoplanktonic organisms in the world oceans.

[3] Coccolithophorids comprise a family of calcite-producing Prymnesiophytes that evolved in the mid-Triassic period [*Lipps*, 1993]. They rose to taxonomic prominence as the primary calcifying organisms following the nannoconid "crisis" at the Cenomanian/Turonian boundary, 93 Ma before present. The accumulation of calcite plates from relict coccolithophorid blooms in the Cretaceous and throughout the Cenozoic represents a significant component of deep-sea oozes and chalks in the open ocean, contributing up to 80% of the total precipitated $CaCO_3$ [*Fabry*, 1989]. There are approximately 200 extant species of coccolithophorids [*Jordan and Green*, 1994], but only two species, *Emiliania huxleyi* and *Gephyrocapsa oceanica*, are known to form seasonal blooms in the present geological period. Of these two bloom-forming species, the more important in the contemporary oceans is *Emiliania huxleyi*. This species forms seasonal blooms that can occupy over 100,000 km^2 of ocean surface [*Brown and Yoder*, 1994], and as such, represents a significant source of biogenically produced calcite in the global oceans [*Westbroek et al.*, 1989].

[4] As the major calcifiers in the open ocean, coccolithophorids alter the equilibrium of the inorganic carbon system and alkalinity of seawater [*Denman and Peña*, 1999]. On timescales shorter than millennia, calcification,

$$Ca^{2+} + 2HCO_3^- \Leftrightarrow CaCO_3 + H_2O + CO_2,$$

leads to a disequilibrium in the carbonate system and potentiates an outgassing of CO_2 to the atmosphere. The system is brought back to steady state by adjustments in the lysocline depth and $CaCO_3$ sediment burial (10^3–10^4 years). On longer timescales (10^6 years), rock weathering restores Ca^{2+} (i.e., alkalinity) to the ocean. As the residence time of Ca^{2+} is $>10^6$ years, short-term changes in the flux of $CaCO_3$ can have significant impacts on the global carbon cycle [*Quay*, 1992; *Heimann and Maier-Reimer*, 1996; *Joos and Bruno*, 1998].

[5] The introduction of ocean color observing satellites in the 1980s facilitated the observations of coccolithophorid blooms from space [*Holligan et al.*, 1983; *Brown and Yoder*, 1994]. These observations were extended by SeaWiFS and MODIS to provide global, synoptic images of the blooms of calcifying organisms [*Brown*, 1999]. Corresponding satellite data sets, in situ climatology, and model fields are also available for key physical, chemical, and biological variables, such as sea surface temperature, solar irradiance, sea height anomalies, surface nutrients, and upper ocean chlorophyll concentrations. The global distribution of these physical variables provides a means to explore the extent to which coccolithophorid blooms detected in satellite imagery, predominantly composed of *E. huxleyi*, can be statistically associated with specific environmental domains. From such analyses, it may be possible to develop a "pseudo-niche" analysis (by "pseudo-niche," we mean that the parameter space we use to define the taxa is based on empirical observations, and, while the parameter may be correlated with the true ecological niche, it is not necessarily a causation of blooms), which uses a suite of critical parameters to define environmental features that select for coccolithophorid blooms. Given one or more sets of preferred parameter spaces, it may be further possible to hindcast and forecast these coccolithophorid blooms in the world oceans. In this paper, our primary goal is to elucidate the parameter space(s) that selects for coccolithophorid blooms on a global scale.

[6] In understanding the factors that result in a bloom of a specific group of organisms, we make the parsimonious assumption that in any given parcel of water in the ocean there is a finite probability of encountering any species of phytoplankton, but that the relative abundance of an individual species is determined by local environmental factors that select for that organism based on its optimal growth potential. This assumption, which we call the "universal distribution, local selection" hypothesis, negates stochastic processes as a causal selective agent. On the basis of this assumption, we present the first description of satellite-detected coccolithophorid populations on a global scale and produce a predictive model of coccolithophorid distribution based upon a conditional probability function using three predictable physical/chemical parameters. We examine changes in the spatial and temporal statistical distribution of

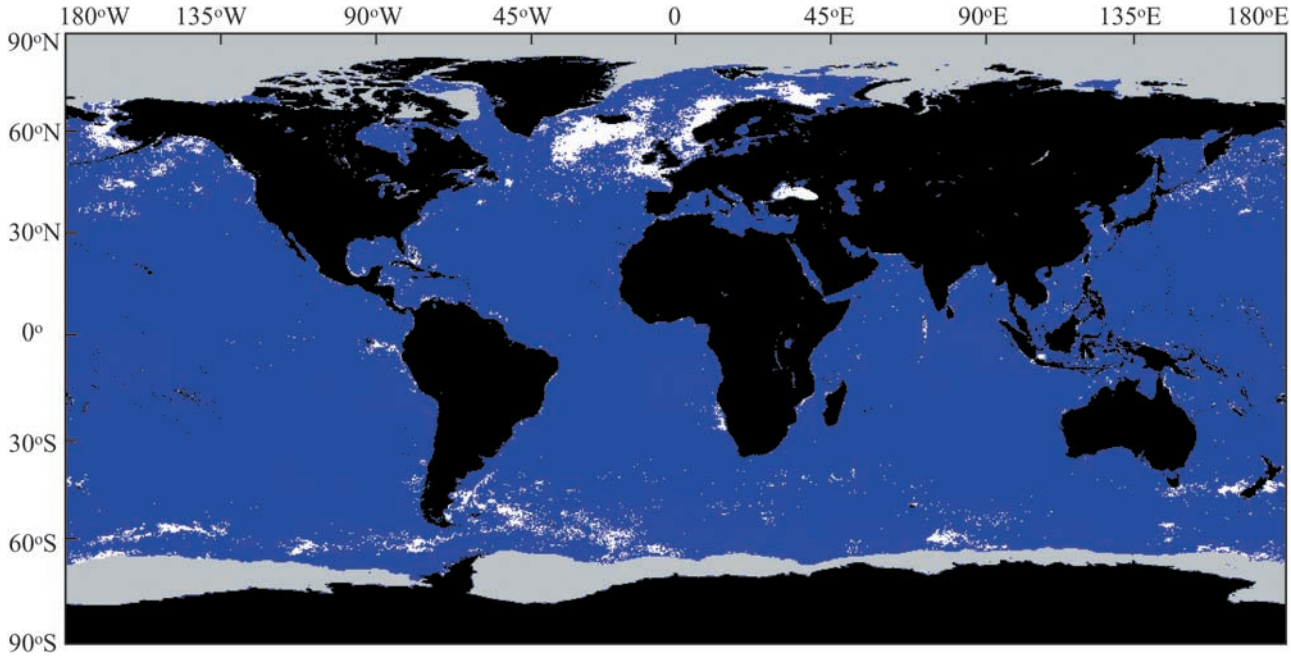

Figure 1. Annual composite of classified coccolithophorid blooms in SeaWiFS imagery dating from October 1997 to September 1999. The bloom class is white, the non-coccolithophorid bloom class is blue, the land is black, and ice is gray.

these coccolithophorid blooms in relation to changes in the chemical and physical dynamics of the ocean with the aim of providing the basis to develop a model that represents coccolithophorids in global biogeochemical cycles and use this information to predict the distribution of coccolithophore blooms in the coming decades.

2. Materials and Methods

2.1. Satellite Data and Methods

[7] The distribution pattern of coccolithophorid blooms in surface waters of the world oceans was mapped by classifying pixels of weekly (8-day) global composites of Sea-viewing Wide Field-of-view Sensor (SeaWiFS) imagery [*McClain et al.*, 1998], dating from October 1997 to September 1999, into coccolithophorid bloom and non-bloom classes using a supervised, multispectral algorithm. (Figure 1). A classified bloom in this study was defined as a detectable entity that possessed spectral characteristics of blooms of the coccolithophorid *Emiliania huxleyi*.

[8] Global images of 8-day mean normalized water-leaving radiances (nLw λ, where λ = 443, 510, and 555 nm) from Level-3 binned SeaWiFS imagery (second reprocessing) were transformed to a cylindrical equidistant projection and subsampled by 2 × 2 decimation to generate an evenly spaced 2048 × 1024 grid with a spatial resolution of approximately 18 km. The Level-3 data, obtained from the NASA GSFC Distributed Active Archive Center, represent averaged geophysical parameters from valid global Level-2 pixels (~4 km resolution) binned to a fixed, linear latitude-longitude array. The imagery was corrected for atmospheric scattering with the default SeaWiFS multiple atmospheric scattering algorithm [*Gordon and Wang*, 1994]. The mean radiance images served as input for the supervised classification algorithm.

[9] The classification algorithm employed was a modified version of the approach developed by *Brown and Yoder* [1994] to detect coccolithophorid blooms in Coastal Zone Color Scanner (CZCS) imagery. Modifications were based upon the spectral signature of *E. huxleyi* blooms observed in Level-2 Global Area Coverage (GAC) SeaWiFS imagery. Spectral signatures were ascertained by extracting normalized water-leaving radiances from pixels located in high-reflectance regions of the Bering Sea, the Celtic Sea, and the central North Atlantic (Table 1) where *E. huxleyi* blooms had been sampled coincidentally or previously [*Holligan et al.*, 1983, 1993; *Vance et al.*, 1998; *Steinke et al.*, 1999]. The following spectral criteria were used to detect *E. huxleyi* blooms: nLw443 > 1.1, nLw555 $\geq$ 0.9, 0.7 < nLw443/nLw510 < 1.1, 0.85 < nLw443/nLw555 < 1.4, and 1.0 < nLw 510/nLw555 < 1.4, with radiances in units of mW cm^{-2} nm^{-1} sr^{-1}. In addition to the spectral criteria, a bathymetric threshold (depth > 100 m) was applied between 45°S and 45°N to reduce the incorrect grouping of shallow carbonate shelves as coccolithophorid blooms. The aerosol

Table 1. Coordinates and Dates of Sites Used to Establish Spectral Signatures for *Emiliania huxleyi* Blooms in SeaWiFS Imagery

Date	Sample Size, pixels	Coordinates
2 April 1998	12,884	58.5°N, 167.6°W
18 May 1998	3241	53.3°N, 12.1°W
18 May 1998	3853	49.7°N, 8.6°W
15 June 1998	2942	62.0°N, 25.5°W

Table 2. Coccolithophorid Abundance[a]

Month	Atlantic	Pacific	Southern Ocean	Arctic	Indian	Global
January	350	382	685	0	77	1494
February	425	183	216	0	47	871
March	364	184	30	0	26	604
April	249	111	0	0	12	372
May	562	142	0	0	17	721
June	6286	704	0	233	46	7269
July	1829	650	1	390	50	2920
August	1006	569	0	1136	78	2789
September	247	478	4	110	58	897
October	144	208	21	0	42	415
November	300	397	90	0	50	837
December	457	296	1309	0	119	2181
Total	12219	4304	2356	1869	622	21370

[a] Numbers represent composites of coccolithophorid occurrence in individual SeaWiFS pixels for each month from October 1997 to September 1999.

radiance criteria (La 670 < 1.10 mW cm^{-2} nm^{-1} sr^{-1}) used by *Brown and Yoder* [1994] was not implemented.

[10] Global monthly data for all variables were arranged on an evenly spaced 2048 × 1024 rectangular grid, from which we produced monthly maps of coccolithophorids and of the climatological variables, globally and for each ocean (see http://marine.rutgers.edu/opp/Mask/MASK1.html for ocean masks).

[11] The abundance (= number of pixels) of classified blooms located from 75°N to 60°S were tabulated from the monthly climatologies for each ocean and globally (Table 2). ''Monthly'' composites were produced by combining sequential classified images in such a way as to display the location of all classified blooms detected during a given month. Classified images were included in a given monthly composite if the initial date of the 8-day image fell within that month. We assume that a classified bloom in a given month represents all stages of bloom development, given that a typical transition from coccospheres (healthy coccolithophorid growing cells) to high coccolith-shedding cells (symptomatic of nutrient-stressed cells) takes place in timescales far shorter than a month [*Balch et al.*, 1992].

[12] These monthly composites were used to produce global annual and climatological composites and to identify the key physical and chemical variables coincident or correlated with the temporal and spatial patterns of coccolithophorids in the upper ocean. The relative importance of each selected variable as predictors of coccolithophorid blooms was investigated using a probability density function for each month for coccolithophorid distributions; i.e., the probability of encountering a pixel containing a classified bloom of coccolithophorids anywhere in the global ocean in any given month.

2.2. Environmental Climatologies

[13] Ten environmental variables (Table 3) were used to assess their relationships to the presence of classified coccolithophorid blooms. Sea surface temperature (SST) maps were obtained from the Integrated Global Ocean Services System (IGOSS). The optimum interpolated SST analysis uses in situ and satellite SST's plus SST's simulated by sea-ice cover [see *Reynolds*, 1988; *Reynolds and Marsico*, 1993]. The satellite observations were obtained from operational data produced by the National Environmental Satellite, Data and Information Service (NESDIS). Chlorophyll data were obtained from SeaWiFS retrievals using NASA's standard Level 3 data product. Mixed layer (Z_m) profiles were computed from the National Center for Atmospheric Research (NCAR) Climate Ocean Model (NCOM) forced with historical atmospheric reanalysis and satellite data for the time period 1958–1997 (S. C. Doney et al., Modeling global oceanic interannual variability (1958–1997): Simulation design and model-data evaluation, submitted to *Journal of Climate*, 2002). From the numerous definitions of mixed layer depth, the following is adopted because it can be applied globally throughout the annual cycle. First, the discrete model profile of buoyancy b_k at depth $-z_k$ is scanned for the maximum of $(b_k - b_1)z_k^{-1}$, where the first level buoyancy b_1 is equated to the surface buoyancy. The mixed layer depth Z_m is then the shallowest depth where the local, interpolated buoyancy gradient first equals this maximum. Buoyancy profiles that are linear and stable to the bottom are assigned $Z_m = -Z_1$. Whenever all deeper buoyancies are greater than or equal to b_1 (unstable), the mixed layer depth equals the depth of the bottom level. Euphotic zone depth (Z_e) is based on satellite surface chlorophyll concentration according to *Berthon and Morel* [1992]. Solar irradiances (E_0) were obtained from the National Geophysical Data Center based on satellite observations.

[14] Monthly climatologies of nitrate, phosphate, and silicate were obtained from the National Oceanographic

Table 3. Climatological Variables

Variable	Symbol	Values	Source
Chlorophyll	Chl	0–52 mg Chl/m^3	SeaWiFs
Salinity	Sal	27–40 p.s.u.	*Levitus* [1982]
Sea surface temperature	SST	0–32°C	IGOSS
Mixed layer depth	Z_m*	0 ≥ 250 m	NCAR
Euphotic zone depth	Z_e*	0–124 m	*Berthon and Morel* [1992]
Irradiance	E_0*	0–72 mol/m2/day	NGDC
East velocity component	U_E	−32–+32 cm/s	NCAR
North velocity component	U_N	−32–+32 cm/s	NCAR
Vertical velocity component	U_v	−64–+64 cm/s	NCAR
Nitrate	N	0–30	NODC
Nitrate* [(N−16P + 2.9) × 0.87]	N*	−6 ± 6 μM	*Gruber and Sarmiento* [1997]
Phosphate	P	0–2 μM	NODC
Silicate	Si	0–≥ 50 μM	NODC

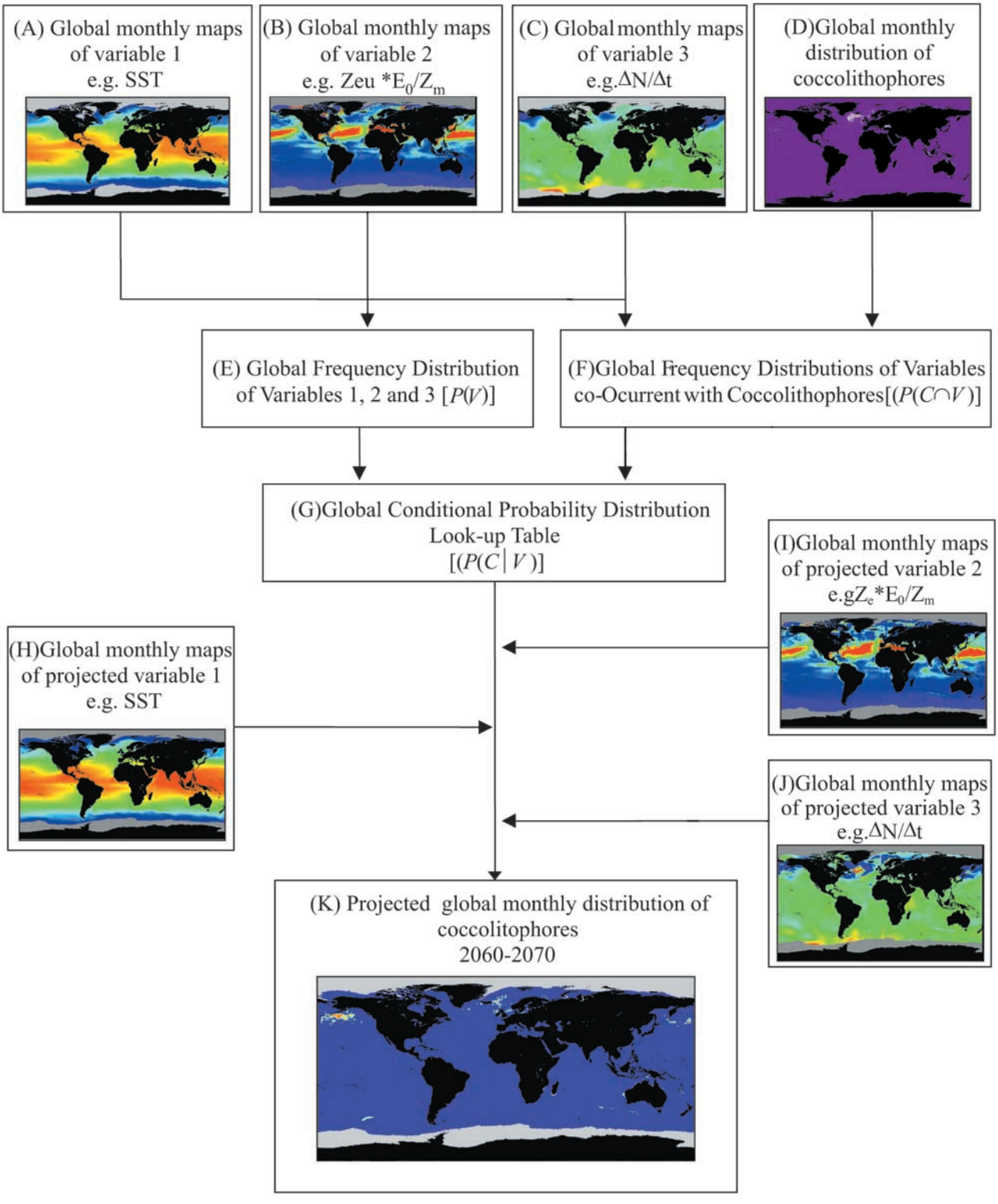

Figure 2. Flowchart representing the protocol to calculate current and projected conditional probabilities. Global maps of SST, E_{cr}, $\Delta N/\Delta t$, and coccolithophorid distribution for June current conditions are represented at the top of the chart. Global monthly unconditional frequency distribution of SST, E_{cr}, $\Delta N/\Delta t$, and global monthly frequency distributions of these variables cooccurrent with coccolithophorids were used to produce the global conditional probability distribution of coccolithophorids.

Data Center (NODC) World Ocean Atlas 1998 data set [*Conkright et al.*, 1998]. We vertically interpolated the data to the mixed layer using the appropriate NODC standard levels (0, 10, 20, 30, 50, 75, 100, 125, 150, 200, 250, 300, 400, and 500 m). A horizontal interpolation was carried out according to *Najjar and Keeling* [1997] and distance-weighted averaging with a 1000-km Cressman function was used to smooth the monthly binned fields.

2.3. Probability Analysis

[15] We generated monthly maps of coccolithophorid climatologies, i.e., pixel abundance for the combined 1997–1998 and 1998–1999 years (Table 2), and for the monthly climatological physical and chemical variables investigated (Table 3). We excluded the Mediterranean/Black Sea region as it is almost entirely represented by the Black Sea bloom. This region has a unique hydrology and has recently been subjected to anthropogenic impact [see *Mihnea*, 1997]; therefore it likely is not representative of open ocean coccolithophorid blooms.

[16] To analyze which of the environmental variables discriminate for coccolithophorids, we calculated conditional probability distributions, $P(C|V)$, that coccolithophorids are present under a given set of conditions, V. To produce the probability distributions, we employed the numerical protocol as described in Figure 2. Using global monthly maps of coccolithophorids, and three selected variables: SST, the ratio ($Z_{eu} \times E_0/Z_m$), or critical irradiance parameter (E_{cr}), and monthly variations in nitrate ($\Delta N/\Delta t$), we calculated the 3-D frequency distributions of the variables co-occurrent with coccolithophorids, $P(C \cap V)$ and normalized them with their unconditional 3-D frequency distributions $P(V)$ to generate a conditional frequency distribution $P(C|V)$ (Figure 2). Only data points with >10 occurrences in the $P(C \cap V)$ histogram were used in this calculation.

[17] Future probability frequency distributions were generated as described in Figure 2. Using the look-up table that describes $P(C|V)$, we projected these probabilities to future climate scenarios (2060–2070) using the same three physical variables (SST, E_{cr}, and $\Delta N/\Delta t$) predicted for 2060–2070 from the NCAR Community Climate System Model (CCSM), a coupled ocean-atmosphere-land-sea-ice model [*Boville and Gent*, 1998; *Blackmon et al.*, 2001]. The future scenario was forced with atmospheric greenhouse gases and aerosols following the Intergovernmental Panel on Climate Change (IPCC) SRES A1 emissions scenario. The CCSM model run for this scenario and the control simulation are available electronically (labeled b030.02, b030.03, and b030.04; see http://www.cgd.ucar.edu/csm/experiments/ for details). To account for interannual variability, we have produced monthly climatologies based on temperature, mixed layer depth, upwelling velocity, irradiance and other properties for the period 2060–2070. This climatology, and a similar one constructed for the control simulation, were used to drive an off-line, global marine ecosystem model [*Moore et al.*, 2001a, 2001b], quantifying the response of biological variables (chlorophyll, nutrients, primary production) to the change in physics. Note that this approach does not capture the effect of long-term trends in upper thermocline nutrient fields.

Table 4. *Emiliania huxleyi* Global Clonal Isolates

Clone	Date of Isolation	Location
B92/11	30 April 1992	North Atlantic
B92/12	30 April 1992	North Atlantic
B92/27	01 May 1992	North Atlantic
B92/28	01 May 1992	North Atlantic
B92/78	07 May 1992	North Atlantic
B92/131	14 May 1992	North Atlantic
B92/43	02 May 1992	North Atlantic
SA	April 1992	Durban, South Africa
NZ	1992	Big Glory Bay, New Zealand

2.4. Amplified Fragment Length Polymorphism Analysis

[18] We used the Amplified Fragment Length Polymorphism (AFLP) approach to analyze genetic variability of *E. huxleyi* populations obtained from various regions in the global ocean. This approach is based upon the selective amplification of a subset of genomic restriction fragments using the polymerase chain reaction (PCR) [*Vos et al.*, 1995]. DNA from selected *Emiliania huxleyi* strains (see Table 4) was digested completely with *Eco*RI and *Mse*I. Double stranded, oligonucleotide adapters were ligated to the ends of the DNA fragments to generate template DNA for amplification. The adapters and the adjacent restriction enzyme recognition sites served as primer binding sites for subsequent amplification of the restriction fragments. Selective nucleotides extending into the restriction fragment were added to the 3'-end of the PCR primers (either G or GA) such that only a subset of the fragments were amplified, i.e., only those fragments in which the nucleotides flanking the restriction site match the selected nucleotides. The size distribution of the amplified fragments was analyzed by denaturing polyacrylamide gel electrophoresis and autoradiography (the *Eco*RI-selective amplification primers were labeled at their 5′-ends with ^{33}P).

3. Results

3.1. Coccolithophorid Distribution

[19] Satellite retrievals from SeaWiFS between September 1997 and January 2000 revealed a typical, annual repeating pattern of coccolithophorid blooms in subpolar latitudes during the summer months, with the largest expanse in the North Atlantic (Figure 1). Three major seasonal coccolithophorid blooms were observed during the Northern and Southern Hemisphere summers between October 1997 and September 1999. These blooms were found in the North Atlantic, the North Pacific (see Figure 3a), and the Southern Ocean (see Figure 3a). In the North Atlantic, three major reflectance areas were identified: one south of Iceland, following the Irminger Current; one west of the United Kingdom shelf waters, following the North Atlantic drift, and one west of Norway, following the Norwegian Current. Additionally, smaller-scale coccolithophorid upper ocean blooms were observed in the subpolar North Atlantic, off the coasts of Florida, south of the United Kingdom, and in the Gulf of Mexico (Figure 1). In the subpolar North Pacific, during the spring of the 1997 El Niño year, instead of the usual dominance of diatoms, a coccolithophorid

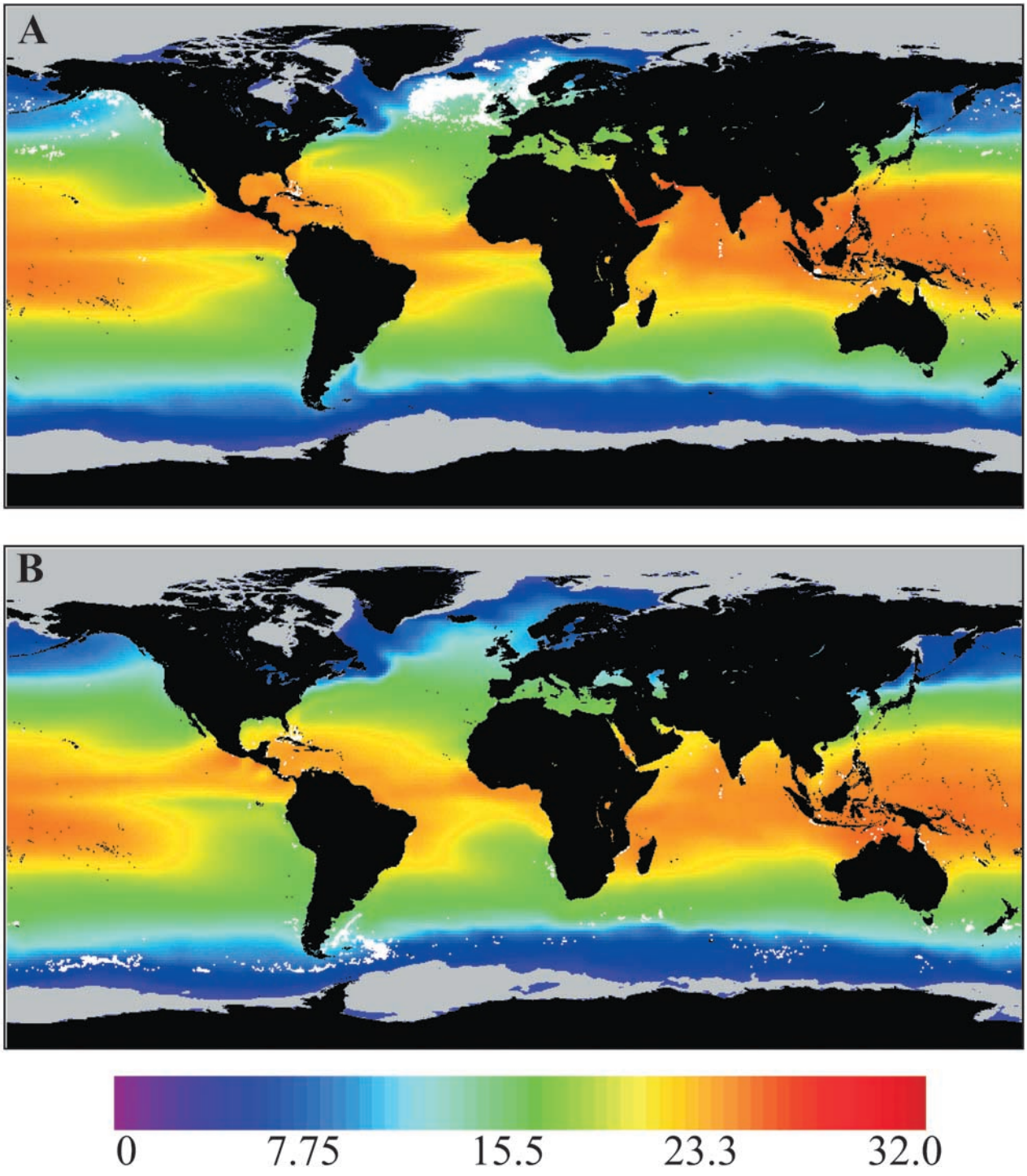

Figure 3. Coccolithophorid climatologies superimposed onto SST climatologies for (a) June and (b) December. Color bars represent SST (°C).

bloom was observed in a large portion of the Bering Sea. SeaWiFS true color images and climatology of classified coccolithophorid bloom observations showed similar coccolithophorid distributions during the spring and summer of 1998 and 1999.

[20] In the Southern Ocean, we observed large aggregations of coccolithophorid blooms forming a belt north of the Antarctic Polar Front (APF) in the Pacific and Atlantic sectors, following the Antarctic Circumpolar Current (Figure 1). It appears to have initiated in the Pacific sector and subsequently moved eastward, with the highest pixel density in the Atlantic and Pacific sectors, north of the APF. Though smaller in areal extent, blooms were also seasonally found in waters off Chile, in the confluence of the Brazil/

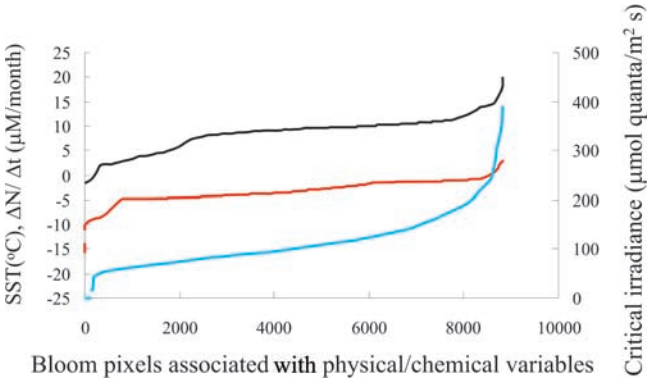

Figure 4. SST (black), E_{cr}, (blue), and $\Delta N/\Delta t$ (red) values associated with coccolithophorid occurrences in the North Atlantic (40°N–75°N), North Pacific (40°N–75°N), and Southern Ocean (40°S–60°S).

Malvinas currents, in the Southern Benguella Current, off the coasts of Australia, south of New Zealand, and off the Galapagos Islands (Figure 1).

3.2. Relationships Between Classified Blooms and Environmental Conditions

[21] The onset of the Northern and Southern Hemisphere classified blooms coincided with a sharp seasonal decrease in the depth of the upper mixed layer (results not shown). In the North Atlantic, the most pronounced changes in Z_m were observed in the northwest Atlantic from 25°N to 75°N and in the central and northeast Atlantic and North Pacific from 45°N to 75°N. In the Southern Ocean, the largest oscillations were observed between 35°S and 60°S, mostly in the Indian and the Pacific Oceans. In both Northern and Southern Hemispheres, the largest blooms were observed where temperatures range between 5° and 15°C (Figures 3 and 4). These areas correspond to the North Atlantic between 48°N and 75°N, with most of the bloom pixels concentrated between 48°N and 64°N, and the Southern Ocean, north of the APF (Figure 3). Most coccolithophorid blooms were observed in waters with salinity values between 33 and 35‰, although sporadic blooms were observed at salinities as high as 39‰ (results not shown), confirming their high threshold tolerance to salinity [*Fisher and Honjo*, 1989]. The highest amplitude in chlorophyll values was observed at high latitudes (results not shown). Chlorophyll *a* concentrations increased sharply prior to the coccolithophorid blooms both in the Northern and Southern Hemispheres (results not shown). This phytoplankton bloom was presumably dominated by other chromophytes, such as diatoms, based on previous field observations.

[22] The distribution of E_{cr} shows its highest amplitude in the high latitudes with values close to zero during the winter months and rising to between 25 and 150 μmol quanta m^{-2} s^{-1} (Figures 4 and 5), whereas low latitudes show relatively high values throughout the year. The largest monthly oscillations in nitrate (Figures 4 and 6), phosphate, and silicate (results not shown) concentrations were observed at high latitudes. A particularly pronounced annual cycle was observed in the North Pacific (north of 40°N) and to a lesser extent in the North Atlantic (north of 50°N), where the highest concentrations were observed during the winter months. The widest range of nitrate values was observed in surface waters of the North Pacific at the Bering Sea (5–25 μM) and at the Sea of Okhotsk (5–30 μM). In the North Atlantic, the largest amplitude was observed in the Labrador Sea (8–14 μM). Overall, Southern Ocean waters are permanently macronutrient replete as a result of iron limitation, deep winter mixing, and high rates of upwelling. During the austral summer, the Southern Hemisphere waters have the highest nitrate values with the greatest amplitude north of the Antarctic Polar Front. The mixed layer average nitrate shows consistently high values between 15 and 32 μM in the Southern Ocean from 50° to the APF (results not shown). Areas of decreasing nitrate concentrations ($\Delta N/\Delta t < 0$) were associated with coccolithophorids (Figure 4), while no relationship could be established between the presence of coccolithophorids and changes in phosphate or silicate (results not shown).

3.3. Probability Analyses

[23] Among the 13 variables tested, we selected three based upon the most localized conditional frequency distribution; that is, we used the variables most discriminative for coccolithophorids presence. We selected the combined variables E_{cr}, $\Delta N/\Delta t$, and SST after full examination of all the three-variable sets with respect to the above criteria. Figures 3, 5, and 6 show Northern (Figures 3a, 5a, and 6a) and Southern (Figures 3b, 5b, and 6b) Hemisphere summer blooms superimposed to SST, E_{cr}, and $\Delta N/\Delta t$, respectively. We mapped the calculated conditional probabilities ($P(C|V)$) into the global distributions of SST, E_{cr}, and $\Delta N/\Delta t$ (Figure 7) for June (Figure 7a) and December (Figure 7b), creating a 3-D look up table for ($P(C|V)$) as a function of the three variables. The highest probabilities were observed in the Northern and Southern Hemisphere's high latitudes between 45°N and 65°N and between 50°S and 60°S, respectively (Figure 7). Comparison of Figures 3, 5, 6, and 7 shows that the estimated geographic probability fields are in good general agreement with the underlying bloom data; that is, high probability in the observed bloom regions with relatively few "false positives" (e.g., moderate values off of Nova Scotia and Newfoundland) predicted blooms where none are observed.

[24] To produce the probability distribution, we employed the numerical protocol as described in Figure 2. We calculated conditional probability distributions, $P(C|V)$ that coccolithophores are present under a given set of conditions, V. Using global monthly maps of coccolithophores (Figure 2d) and the selected variables (Figures 2a, 2b, and 2c), we calculated the 3-D frequency distributions of the variables co-occurrent with coccolithophores, $P(C|V)$ (Figure 2f), and normalized them with their unconditional 3-D frequency distributions $P(V)$ (Figure 2e). Only data points with >10 occurrences in the $P(V)$ histogram were used in this calculation. The resulting conditional frequency distribution (Figure 2g) constitutes the probability look-up table. Using this look-up table and projected variables (Figures 2h, 2i, and 2j), we generated projected global monthly probability maps of coccolithophorid occurrence for the years 2060–2070 (Figure 2k).

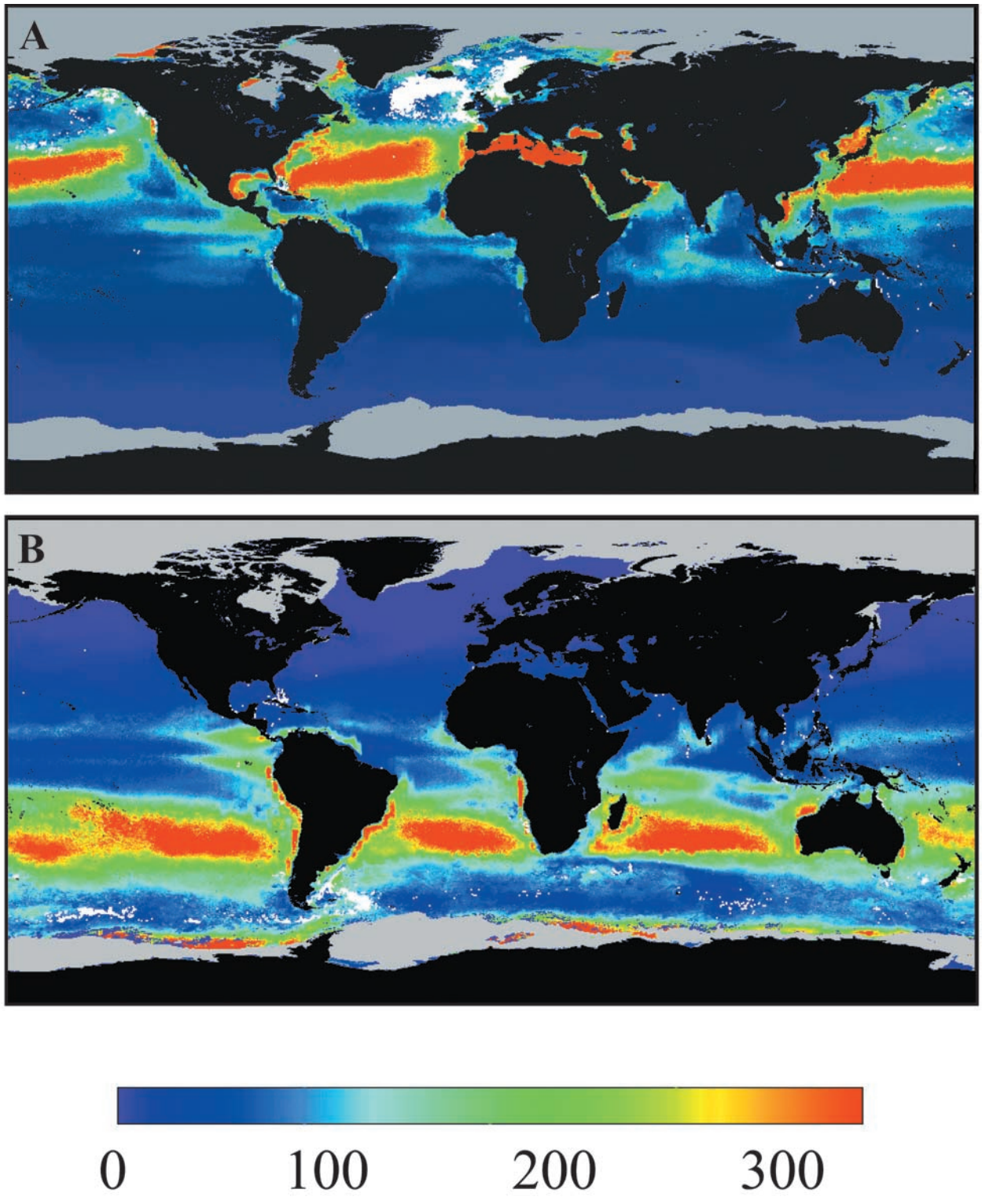

Figure 5. Coccolithophorid climatologies superimposed onto E_{cr} climatologies for (a) June and (b) December. Color bars represent E_{cr} (μmol quanta/m^2/s).

[25] To analyze the future trends in coccolithophorid populations in the world's ocean, we compared the present probability distribution of coccolithophores (Figure 7) with the projection for June and December of 2060–2070 (Figures 8 and 9). The projected warming in SST from the future (2060–2070) minus control scenario is largest in the subpolar North Atlantic, followed by the subpolar North Pacific and then the Southern Ocean (Figure 9). Complex patterns of

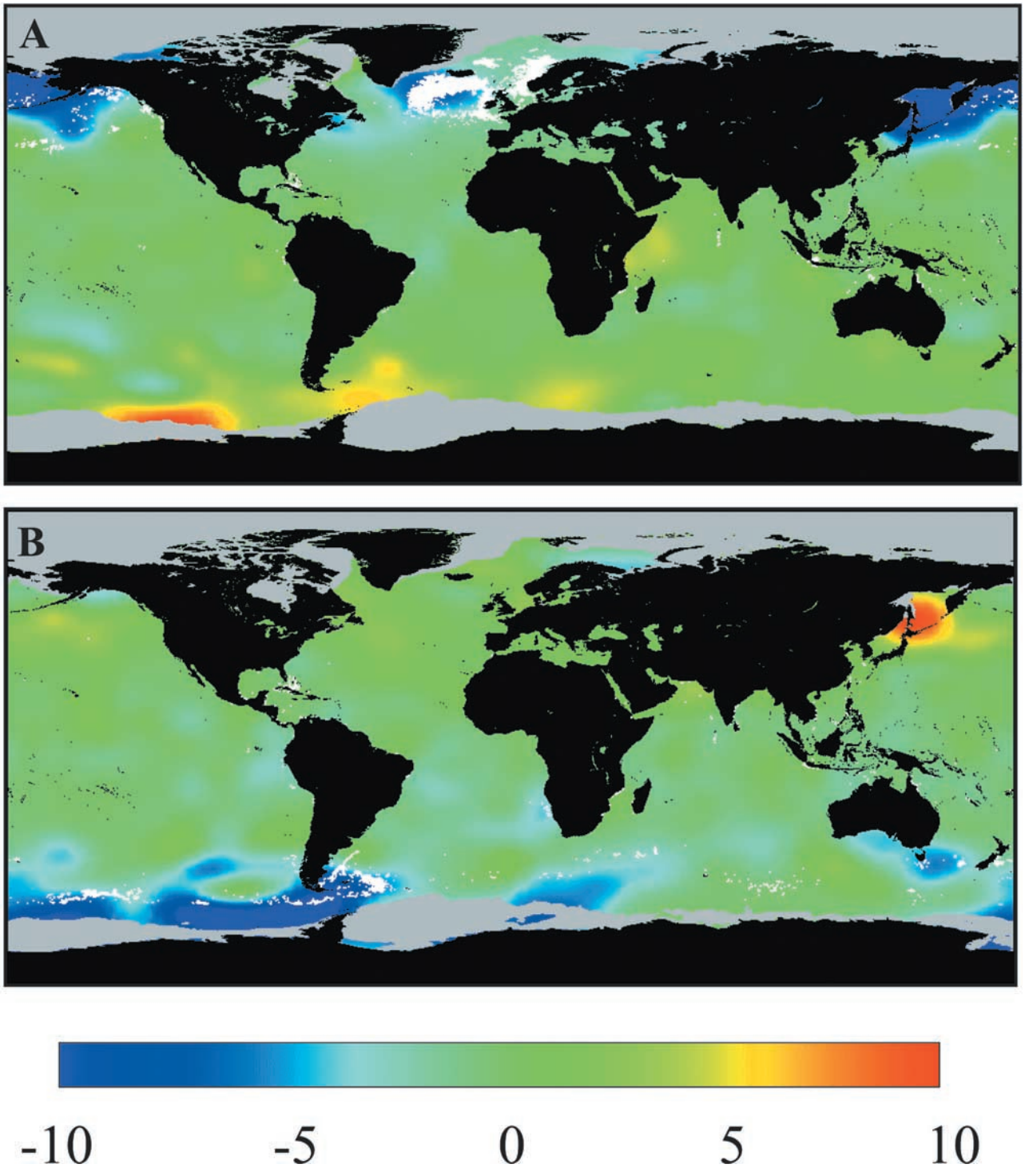

Figure 6. Coccolithophorid climatologies superimposed onto $\Delta N/\Delta t$ climatologies for (a) June and (b) December. Color bars represent $\Delta N/\Delta t$ (μM/month).

changing E_{cr} are found in the subpolar gyres, a combination of sea-ice retreat, changes in mixed layer depth patterns, and biological response. The change in coccolithophorid occurrence in the Northern Hemisphere appears to be mostly driven by changes in $\Delta N/\Delta t$ in the North Atlantic, where projected $\Delta N/\Delta t$ alters by as much as 10 μM/month, from current values of −4 to 0 μM/month observed in coccolithophorid bloom areas. The Pacific and Southern Ocean projected $\Delta N/\Delta t$ remains mostly unchanged (Figure 9). The predicted SST values are higher for all three analyzed oceans, with the greatest increase in the North Atlantic. This increase may additionally contribute to changes in coccoli-

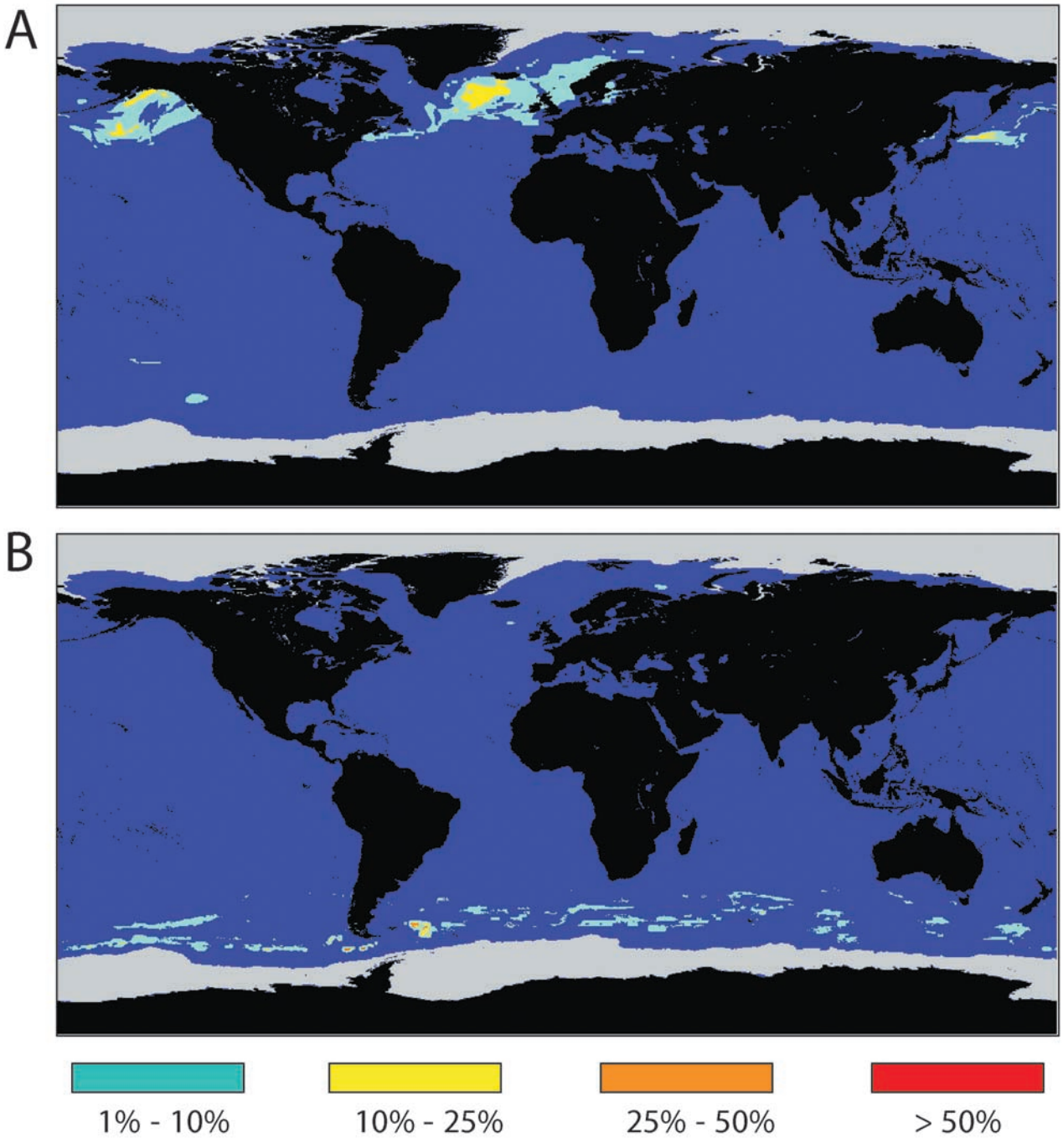

Figure 7. Global conditional probabilities of coccolithophorid bloom presence for (a) June and (b) December based upon their conditional probability distribution [$P(C|V)$] and global monthly SST, E_{cr}, and $\Delta N/\Delta t$.

thophorid occurrence in this region. E_{cr} decreases slightly in the lower range of its values while the higher values remain constant in the North Atlantic and Pacific. The projected critical irradiance increases slightly in the Southern Ocean (Figure 9c).

[26] Our calculations suggest that the projected Northern Hemisphere probability frequencies are lower than under current ocean conditions (see Table 5 and Figure 10). In the Northern Hemisphere, the North Atlantic shows the most dramatic decrease in the size of the probability frequencies, whereas the North Pacific shows a decrease in areal extent and an increase in maximum probability values. In the Southern Hemisphere, probability frequencies decrease slightly (5%) (Table 5). Accordingly, we estimate that the area of surface blooms of coccolithophorids will decrease by up to 50% in the Northern Hemisphere and by 5% in the Southern Hemisphere within this century (Table 5).

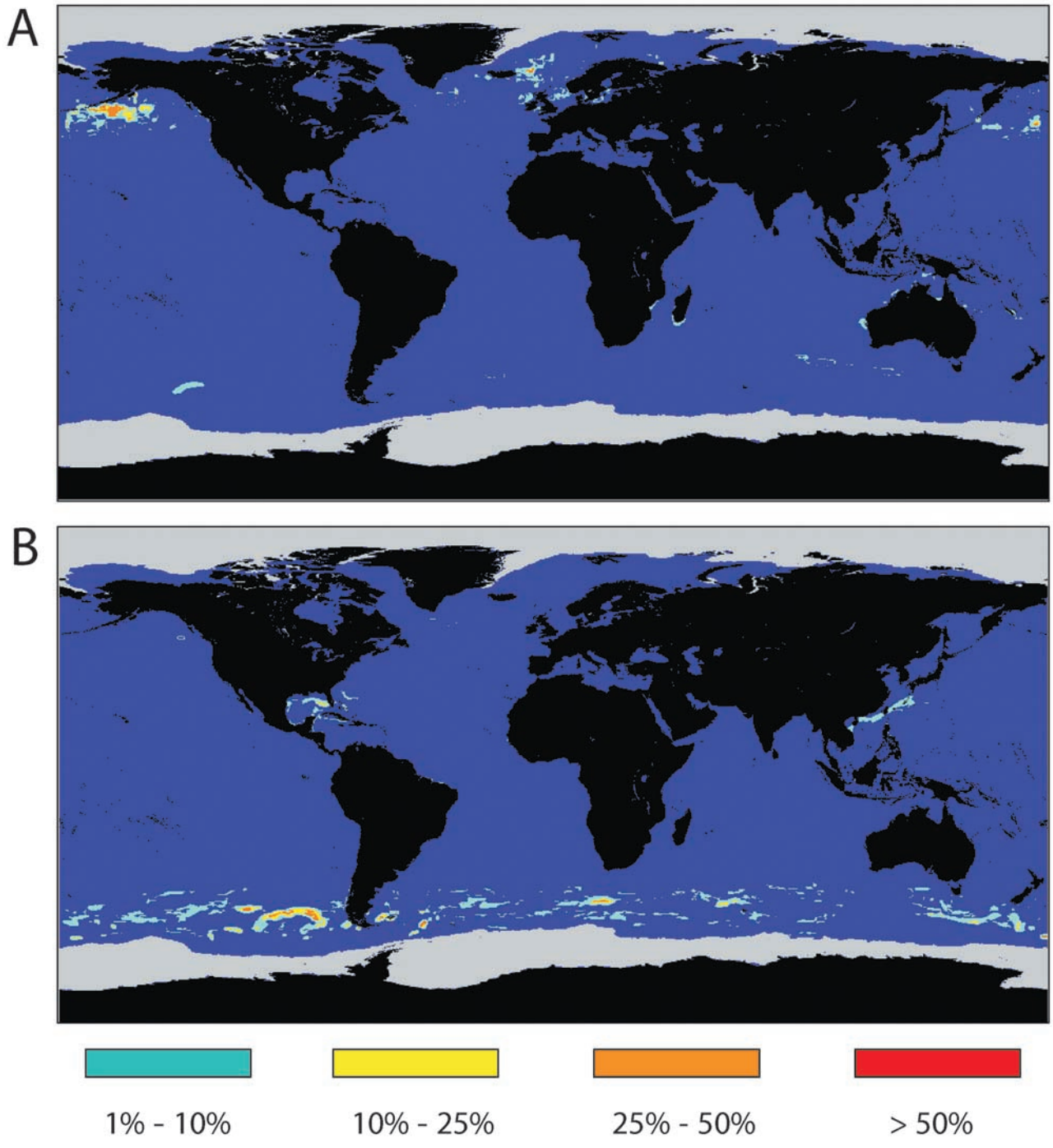

Figure 8. Projected global conditional probabilities of coccolithophorid bloom presence for (a) June and (b) December based upon the probability look up table using projected SST, E_{cr}, and $\Delta N/\Delta t$ climatologies.

[27] These projections should be considered as illustrative given the considerable variation and uncertainty in coupled model results. While the large-scale patterns of future climate change (e.g., warmer SSTs, increased stratification) are robust across all current models, the magnitude and regional patterns vary widely. Overall, the CCSM climate sensitivity tends to fall on the low side. The large amplitude changes observed in the model North Atlantic subpolar gyre (which drives the predicted decline in coccolithophorids) are due to a melt back of sea-ice, which is overly extensive in the control simulation. Additionally, our model does not include the potential decrease in calcification arising from the acidifica-

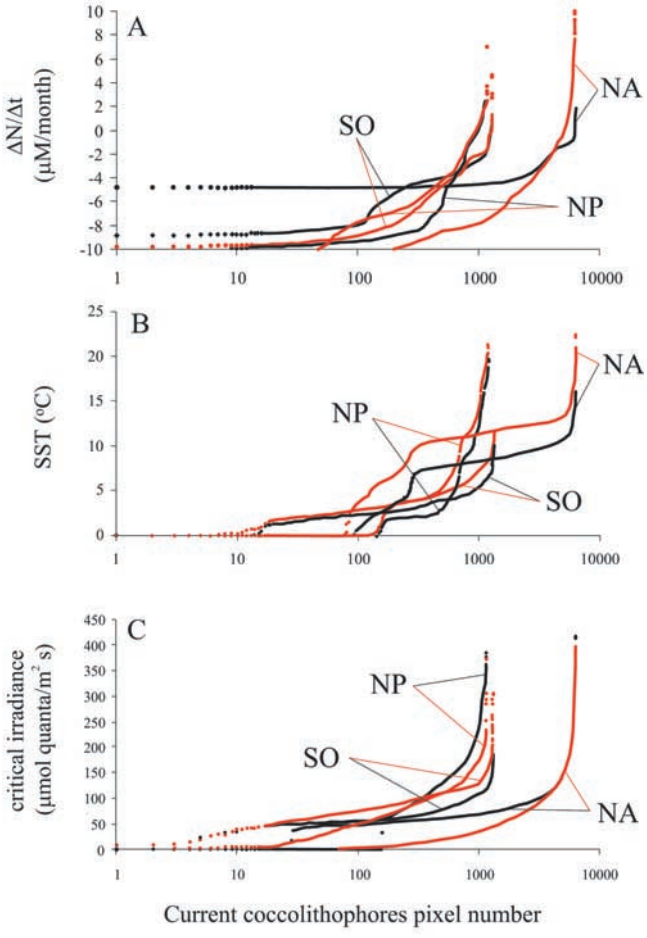

Figure 9. ΔN/Δt, SST, and E_{cr} in coccolithophore bloom areas (black) and projected values for 2060–2070 (red) in the same areas.

tion of the upper ocean as atmospheric CO_2 levels increase [*Riebesell et al.*, 2000].

3.4. Analysis of Genetic Diversity

[28] An analysis of the AFLPs banding pattern reveals significant genetic diversity within *E. huxleyi* (Figure 11). AFLP profiles for a selection of global isolates, a series of North Atlantic isolates forming a time series through a Norwegian mesocosm bloom and two clones from Southern Hemisphere waters (off the coasts of New Zealand, NZ, and South Africa, SA), show that no two clones share an identical genotype (results not shown). The complex banding patterns were analyzed by scoring the presence/absence of each size fragment in each *E. huxleyi* clone and then calculating Jaccard's coefficient to give a measure of genetic distance. The distance matrix was analyzed by UPGMA in PHYLIP and the tree file plotted as a phylogram using TreeView (Figure 11a). The distances between the *E. huxleyi* clones were rather small; 78 out of the 99 amplification fragments were present in all the 9 clones investigated. All but two clones (12 and 78) from a single Norwegian mesocosm appear to have a unique genotype. These mesocosm clones form a single sister clade to two geographically distinct isolates (NZ and SA).

4. Discussion

4.1. Biogeography of Coccolithophorids

[29] This is the first study providing monthly global representations of a specific phytoplankton functional group in a statistical, diagnostic model. Among all the variables tested, $\Delta N/\Delta t$, critical irradiance, and SST showed the closest correlation with the presence of coccolithophorids, and among these, $\Delta N/\Delta t$ appears to explain most of the variance (up to 50%) of $P(C|V)$. Our results reveal that although coccolithophorid populations are cosmopolitan, the large-scale, seasonal blooms detected in SeaWiFS imagery are confined primarily to nutrient-depleted, temperate, and high-latitude oceans with relatively high critical irradiances.

[30] The conditional probability look-up table, generated using the monthly climatologies of SST, E_{cr}, and $\Delta N/\Delta t$, represents a significant improvement in our ability to quantify the probability of encountering a pixel containing a bloom of coccolithophorids anywhere in the ocean for any given month. Considering there are 1,374,065 ocean pixels in our rectangular projections, the unconditional probability of randomly encountering a "bloom" pixel of coccolithophorids at any location varies between 0.03 and 0.53% for the months of April and June, respectively (see Table 2). In comparison, the conditional probability in the bloom regions was typically 1–25%, a more than 2 orders of magnitude improvement using the discriminative variables. When pixels are clustered into larger bins, the probability indices can be increased further, with an obvious sacrifice of spatial resolution.

[31] Our results compare with previous in situ observations of *E. huxleyi* and *G. oceanica* blooms and have improved previous investigations using remote sensing to

Table 5. Probabilities for Current and Projected Conditions

Probability	June Current	June Projected	June Projected-Current	December Current	December Projected	December Projected-Current
1–10%	11662	7338	−4324	22086	19099	−2987
11–25%	4258	1309	−2949	1614	2384	770
26–50%	2777	1013	−1764	287	1235	948
>51%	812	120	−692	96	65	−31
Total	19509	9780	−9729	24083	22783	−1300
Surface	6320916		0,501307[a]	7802892		0,94602[a]
Total × 324 m^2		3168720			7381692	

[a] Maximum potential projected:current surface ratio calculated as the product of pixel number by pixel surface area (18 × 18 m^2).

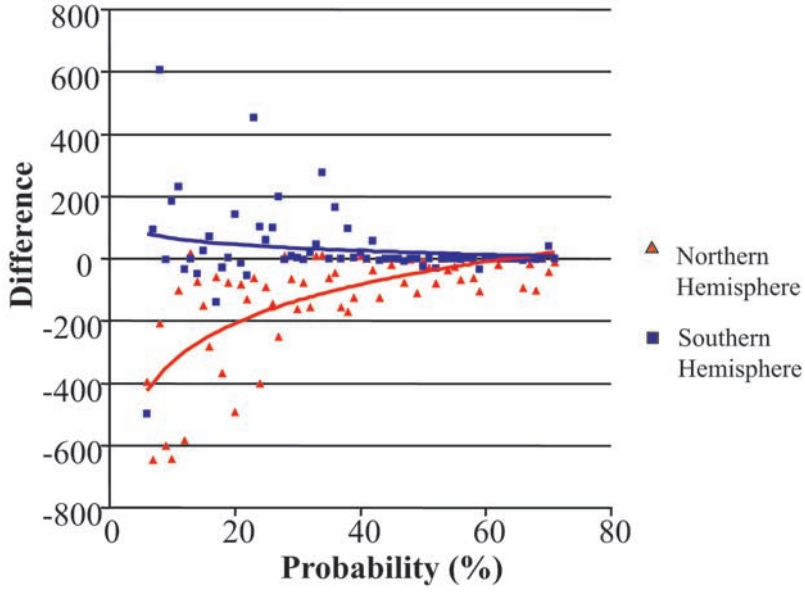

Figure 10. Difference between projected and current probability density functions of coccolithophorid occurrence in the Northern and Southern Hemispheres (June and December, respectively.)

determine their distribution pattern. For example, we have reduced the number of likely misclassified coccolithophorid pixels in several ocean regions by applying a bathymetric threshold compared with observations by *Brown and Yoder* [1994]. In our study, blooms were uncommon or absent in the Persian Gulf, and Indonesian-northern Australian waters during the entire period examined and in the western North Atlantic in 1997–1998. These regions are not known to harbor coccolithophorid blooms, although were categorized as bloom regions in CZCS imagery [*Brown and Yoder*, 1994] because they typically possess shallow (<100 m) calcareous sediments. The classified pixels located in the Gulf of Mexico and around the Bahamas are likely the result of this and suggest that the bathymetric map employed (within SeaDAS) is incorrect.

[32] Classification of these blooms, though relatively robust compared to remote sensing identification of other phytoplankton taxa, has limitations. The detection of coccolithophorid blooms in this study is dependent upon light backscattered from approximately one attenuation depth in the water column and is primarily a function of coccolith, not cell concentration [*Balch et al.*, 1991]. Although *Emiliania huxleyi* is part of the highly diverse low latitudinal coccolithophorid populations, these are often dominated by coccolithophorid species other than *E. huxleyi* that do not shed coccoliths, rarely occur as blooms, live below 50 m depth, and are, therefore, not manifested in a surface optical signature. Our study does not account for nonbloom populations of coccolithophorids, largely representative of tropical and subtropical regions. Satellite images of upper ocean, broad spectrum scattering associated with coccolithophorid blooms could potentially be interpreted as senescent cells, resulting from the detachment of coccoliths. In *Emiliania huxleyi,* this phenomenon is most pronounced at the end phase of a bloom. However, the transition to a rapid increase in coccolith detachment measured in laboratory [*Balch and Kilpatrick*, 1993], mesocosm [*Westbroek et al.*, 1993] and field [*Garcia-Soto et al.*, 1995] experiments is relatively short, occurring on timescales of several days or a few weeks. Given that any classified bloom corresponds to at least one occurrence during that particular month, they represent several, integrated stages of bloom development. While these inherent limitations of remote sensing of a specific phytoplankton functional group should not be ignored, they are offset by quasisynoptic global observations that are only accessible through space-based observations.

[33] The extensive coccolithophorid blooms south of Iceland and in the high-latitude regions in the Atlantic were first reported from satellite imagery [*Brown and Yoder*, 1994; *Holligan et al.*, 1993], but curiously, blooms of these organisms in the Antarctic have been poorly documented. The reports for the North Atlantic were greatly facilitated by CZCS imagery, which had poor coverage of the Southern Hemisphere oceans in general, and the Southern Ocean in particular. In fact, *E. huxleyi* was first reported in the Antarctic waters by *Hentschel* [1932], and subsequently by *McIntyre and Bé* [1967], who described monospecific *E. huxleyi* populations south of the APF. More recently, *Hallegraeff* [1984], *Thomsen et al.* [1988], *Blackburn and Cresswell* [1993], *Eynaud et al.* [1999], *Winter et al.* [1999], *Findlay and Giraudeau* [2000], and S. Honjo et al. (personal communication, 2001) described coccolithophorids in Antarctic waters as far south as 70°S. These reports and our satellite retrievals suggest that the waters immediately north of the APF can support circumpolar blooms of coccolithophorids, and that these organisms can successfully compete with diatoms during the Austral summer. How is this competition related to the physical proxies we adopted to generate our probability analyses?

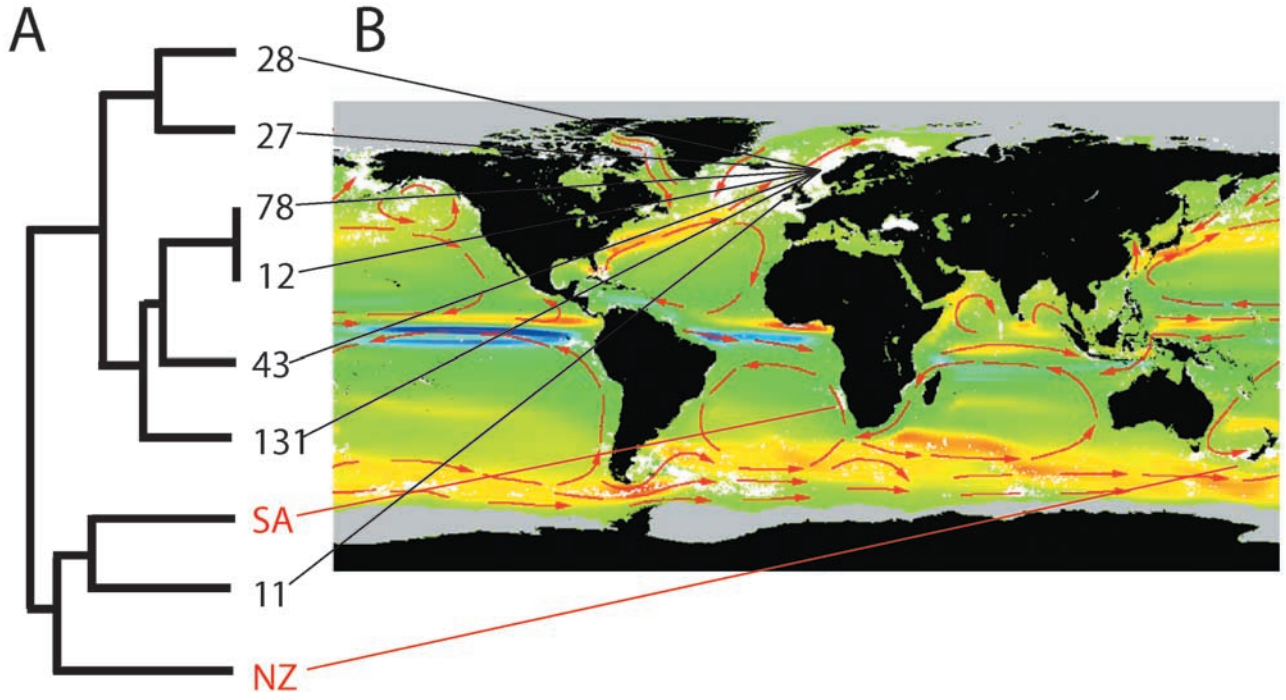

Figure 11. Use of AFLP to distinguish between clonal isolates of *Emiliania huxleyi*. (a) A phylogram showing the relationships between individual clones derived by UPGMA analysis of Jaccard's distances calculated from the band profiles. The distance matrix was analyzed by UPMGA in Phylip and the tree file plotted as a phylogram using TreeView based upon the size distribution of genomic fragments amplified from nine *E. huxleyi* clonal isolates: B92/11, B92/12, B92/27, B92/28, B92/78, B92/131, B92/43, NZ, and SA. (b) Map illustrating the annual global distribution of coccolithophorids in white superimposed onto the East water velocity component. Color bar shows the East water velocity component in cm/s.

[34] While silicate availability is clearly a factor that can limit the distribution of diatoms, coccolithophorids and diatoms compete when silicate is abundant. Diatoms usually prevail under high nutrient (i.e., NO_3^- and PO_4^{2-}) conditions earlier in bloom progression, while coccolithophorids tend to become relatively more abundant and persistent as nutrients become limiting. Coccolithophorids have an exceptionally high affinity for dissolved inorganic nitrogen and phosphate [*Eppley et al.*, 1969] with half-saturation constants for these nutrients being approximately half that of diatoms of comparable size. In contrast, diatoms have relatively high nutrient uptake capacities, rapidly taking them up and hoarding nutrients when abundant. One ecological explanation for the competitive exclusion between the two taxa is based on cellular design. Diatoms devote a relatively large fraction of their cell volume to storage vacuoles. Vacuoles permit excess, i.e., "luxury" uptake [*Ketchum*, 1939] that allows this group to rapidly deplete macronutrients and to provide a reservoir of internally stored nutrients that permits several cell divisions without the need to access external nutrient sources. This "boom and bust" strategy comes at a price; diatoms have relatively low affinities for nutrients. Hence, diatoms are generally selected under relatively unstable environments, where intermittent physical forcing, such as storm-induced mixing events or eddies, can facilitate pulsed nutrient supplies. Coccolithophorids are, on the other hand, small, and lack true storage vacuoles, but have high affinities for nitrate and phosphate [*Eppley et al.*, 1969; *Riegman et al.*, 2000]. This group has selected a "just in time" nutrient supply strategy; that is, in contrast with diatoms, where growth rates are buffered by internal nutrient sources, in coccolithophorids growth rates are directly coupled to external nutrient supplies. Indeed, under nutrient limiting conditions, coccolithophorids out compete diatoms [*Egge and Aksnes*, 1992].

[35] A persistent pattern in our monthly observations is that coccolithophorids bloom when the water column becomes stable. The presence of coccolithophorids in areas of decreasing nitrogen concentration (Figure 6) is supported by in situ observations suggesting that in the North Atlantic, Pacific, and Southern Oceans, these organisms bloom following a sharp increase in water stratification during the summer (results not shown). On the basis of the monthly changes in Z_m, chlorophyll, and the results obtained in the probability analysis, we suggest the following course of events: (1) The modern distribution of satellite detected coccolithophorid blooms is associated with areas of low turbulence; (2) coccolithophorids are associated with semioligotrophic conditions, with blooms being closely associated with areas of decreasing nitrate concentrations; and (3) the three major driving forces that determine the prevalence of coccolithophorid blooms versus blooms of other marine phytoplankters are the stability of the water column, high incident irradiance, and relatively low nutrient concentrations.

[36] On ecological timescales, the effects of turbulence and nutrient supply appear to have altered the dynamic equilibrium between coccolithophorids and nutrient supply in two oceanic areas, namely the Black Sea and the Bering Sea. The sedimentary record reveals that *Emiliania huxleyi* first "invaded" the Black Sea about 1600 Ma before present [*Hay et al.*, 1991]; indeed, the upper laminated sediments of this basin are carbonate rich. There is evidence however, that human activities have altered the biogeochemistry of the Black Sea, skewing the phytoplankton composition toward coccolithophorids. Prior to dam construction on the Danube and other rivers that deliver nutrients to the basin in circa 1970, the phytoplankton community was balanced with diatoms and dinoflagellates [*Mihnea*, 1997]. An exhaustive analysis of the phytoplankton community structure of the Black Sea between 1979 and 1994 shows that *Emiliania huxleyi* was present in bloom concentrations [*Humborg et al.*, 1997; *Mihnea*, 1997]. It has been suggested that the dam construction resulted in a significant decline in the silicate concentration, as the Danube river is responsible for over two thirds of the river inputs into the Black Sea [*Humborg et al.*, 1997]. However, the geological success of *E. huxleyi* in the Black Sea, with a salinity of ca. 18‰ and relatively low nutrient inventories, suggests that the general profile derived for this taxa on the global scale will function on a regional scale as well.

[37] In the eastern portion of the Bering Sea, a large-scale coccolithophorid bloom, instead of the usual diatom dominated system, was reported for the first time during the summer of the 1997 El Niño year. Similar situations occurred during the summers of 1998 and 1999. This change in the phytoplankton community structure is possibly due to sudden alterations in the climate pattern of the North Pacific attributable to the Pacific Decadal Oscillation [*Trenberth*, 1990], in which a more stable water column led to lower surface nutrients and resulted in a shift from a large diatom bloom to a small diatom bloom followed by a large coccolithophorid bloom.

[38] The appearance of satellite-detected coccolithophorid blooms in high-latitude oceans, and the relative paucity of such blooms in the tropics, does not always reflect the spatial patterns of calcite deposition in marine sediments. The spatial biogeochemical shifts between opal and carbonate reflect areas of different productivity regimes [*Pondaven et al.*, 2000; *Sarmiento et al.*, 2002]. The accumulation of calcite in surface sediments is dependent upon biotic and abiotic processes including grazing, dissolution processes, depth of the lysocline, and transport by ocean currents. Perhaps the most pronounced spatial variation in surface calcification is illustrated by Honjo et al. (personal communication, 2001), who report on sediment trap data for the Southern Ocean along 170°W. Their data reveal high carbonate:opal ratios north of the APF reflecting coccolithophorid dominance [*Honjo*, 1997], whereas this ratio decreases dramatically south of the APF, where diatoms often dominate the phytoplankton community. Similarly, the relative abundance of coccolithophorids in the geological past can be obtained from the sediment record where coccolithophorid-dominated areas show $Si_{bio}:C_{inor}$ ratios $\ll 1$ compared to diatom-dominated areas with $Si_{biol}:C_{inor} \gg 1$ [*Honjo*, 1997; *Falkowski et al.*, 1998]. Honjo et al. (personal communication) suggest that at the APF and latitudes further south, more than half of the inorganic carbon originates from pteropod shells and the remaining fraction is represented by planktonic foraminifera. North of the APF the calcite flux is dominated by coccolithophorids.

4.2. Evolutionary Success of Coccolithophorids in the Geological Past

[39] Calcareous nannoplankton appeared for the first time in the Late Triassic, showing great abundance in high latitudes with a peak in diversity during the Late Cretaceous [*Bown and Young*, 1997]. Several mass extinction periods affected the diversity of calcifying nannoplankton, the most pronounced being at the Cretaceous/Tertiary boundary, when approximately 90% of the calcifying nannoplankton taxa became extinct. In the ensuing Cenozoic epoch, diatoms rose to taxonomic prominence among the eucaryotic phytoplankton, a role these organisms enjoy to the present time. What fundamental process(es) determines the relative abundance of coccolithophorids or diatoms in the global oceans?

[40] One major factor that can influence the competitive selection of one of these groups is upper ocean turbulence. High concentrations of coccoliths are found in interglacial sediments, whereas glacial sediments are relatively poor in biogenic carbonate [*Henrich*, 1989]. One example is transitions between glacial-interglacial periods that are evident in the equatorial Atlantic, where decreasing concentrations of coccoliths during glacial periods are thought to be associated to the deepening of the thermocline [*Kinkel et al.*, 2000]. These global scale observations relate to differences in the physiological plasticity of two key eucaryotic phytoplankton functional groups, coccolithophorids and diatoms, and in their ability to cope with physical disturbance. From an evolutionary perspective, these strategic advantages might have been accentuated during glacial-interglacial transitions, when strong selection pressure is exerted. It is therefore fair to assume that the mid-Cenozoic, when there was an expansion of Arctic and Antarctic ice caps forcing sea level changes, and high winds, high mixing, and recycling of nutrients from the bottom layers, did not favor coccolithophorid proliferation and that their ecological niche was threatened by diatoms. We argue that the cellular strategies of diatoms and coccolithophorids, the presence of nutrient vacuoles and high nutrient uptake capacity in diatoms [*Grime*, 1979; *Raven*, 1997], and lack of storage vacuoles and low nutrient uptake rates in coccolithophorids [*Eppley et al.*, 1969; *Riegman et al.*, 2000] may explain the glacial-interglacial transition in the relative abundance of carbonate/silicate deposited in marine sediments above the lysocline. This physical disturbance hypothesis proposes that diatoms are selected when turbulent mixing and pulsed nutrient inputs into the euphotic zone are high, while coccolithophorids are selected under relatively quiescent conditions when nutrient fluxes are low (Figure 12).

4.3. Coccolithophorid Genetic Diversity

[41] In the Cretaceous period, coccolithophorids were extremely abundant throughout the oceans, and diversity

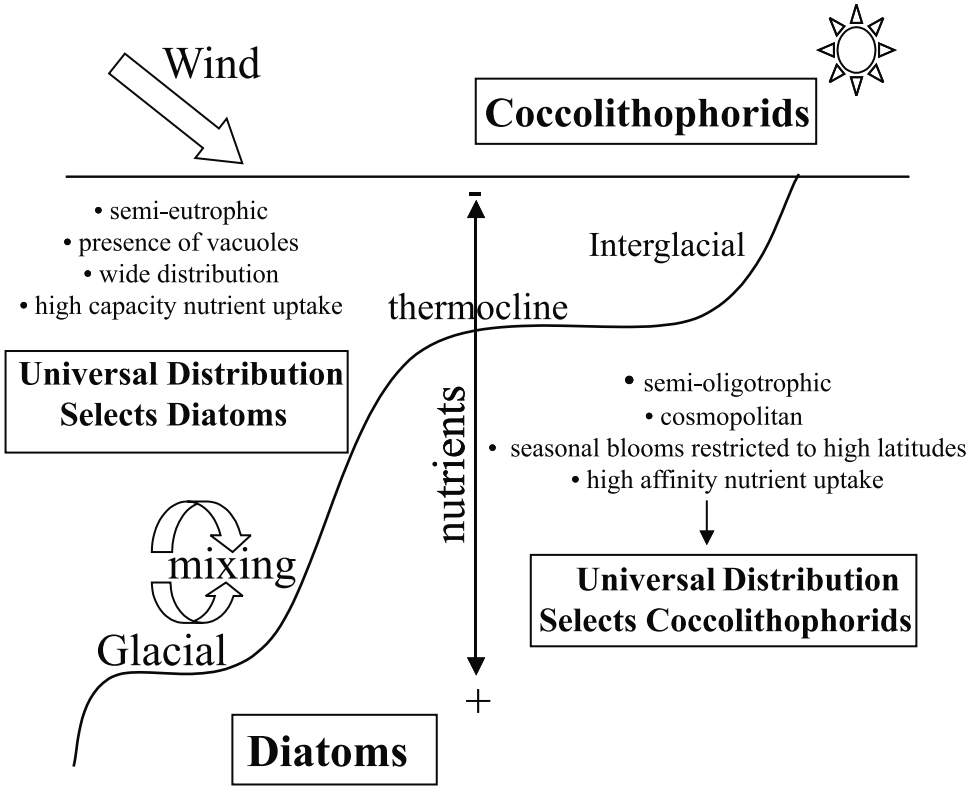

Figure 12. Diagram representing ecophysiological adaptative strategies of coccolithophorids versus diatoms. A glacial scenario (left), characterized by high mixing regimes and semieutrophic conditions selects for diatom populations, with a cell structure and physiological apparatus adapted to physical instability. An interglacial scenario is illustrated on the right-hand side of the figure, characterized by seasonal stratification that allows coccolithophorids to dominate under semioligotrophic conditions as a result of their high affinity for nutrient uptake.

of the group was high. In contrast, in the contemporary ocean, there are only two bloom-forming species. How does a single species, such as *E. huxleyi*, bloom in both hemispheres and under such widely differing environmental conditions? One possibility is that the organism maintains a high degree of physiological plasticity through genetic variation.

[42] Comparative studies at the species and subspecies level indicate that many features known to be homologous within species have diverged in their morphogenetic or physiological underpinnings. For example, the physiological plasticity of coccolithophorids has been demonstrated in *E. huxleyi*, for which environmental conditions appear to determine metabolic responses in clonal isolates of the organism [*Paasche et al.*, 1996]. Three different morphotypes of *E. huxleyi* have been identified [*Hiramatsu and De Deckker*, 1996]; there is temperature-dependent growth rate in *E. huxleyi*, and serological affinity [see *Wood and Leatham*, 1992]. Additionally, certain physiological features are characteristic of particular ecotypes or genotypes [*Malin et al.*, 1992; *Wolfe et al.*, 1994; *Findlay and Giraudeau*, 2000]. Genetic analyses of *E. huxleyi* suggest that there is a significant degree of genetic diversity within this species [*Watabe and Wilbur*, 1966; *McIntyre and Bé*, 1967; *Young and Westbroek*, 1991; *Wood and Leatham*, 1992; *Young*, 1994; *Barker et al.*, 1994; *Medlin et al.*, 1996; *Paasche et al.*, 1996]. This genetic diversity is a direct manifestation of the "Red Queen" process of mutation/selection pressures that maintain fitness in pace with changes in ocean physical forcings on evolutionary timescales.

[43] Our preliminary AFLP data strongly suggest genetic isolation between Northern and Southern Hemisphere populations. Ocean zones such as the Antarctic Convergence, Gulf Stream, and Kuroshio Current are strong barriers to dispersal. Although absence of detectable genetic differentiation does not prove that differentiation is not present, we have identified at least two major lines associated to the Northern and the Southern Hemispheres, that may suggest the possibility that the Northern and Southern Hemisphere coccolithophore populations are evolving separately, potentially leading to new subspecies (see Figure 11), as a consequence of genetic isolation. Indeed, satellite imagery, genetic analyses, and ocean circulation patterns suggest that the North Atlantic clade is seeded by populations originating off the northwest coast of Africa, which are transported by the North Equatorial Counter Current, entrained in the Brazil reflection, and thence carried north toward Iceland and Norway by the Gulf Stream. This distribution pattern has a very low probability of interacting with the circumpolar clade north of the APF in the Southern Hemisphere.

[44] Overall, the relationships revealed by this analysis suggest genotypic variability within the species concept of *E. huxleyi* from geographic locations with distinct hydrographic characteristics. Hence, coccolithophorids such as *E. huxleyi* can be considered widespread taxa but with phenotypes selected by environmental pressures and provided by genetic variation. This process that we call "universal distribution and local selection" has important implications in the flexibility of phenotypic acclimation and genetic adaptation of coccolithophorids to changing environmental conditions. Therefore, while large-scale coccolithophorid blooms are associated with high latitudinal ocean regions, the coccolithophorid group cannot be associated to any particular ecological niche per se, but rather has evolved differently as a function of the evolutionary success of individual subpopulations. In this sense, the species concept within the coccolithophorid community may need to be redefined given the great deal of genetic and physiological plasticity of *E. huxleyi*. What we refer to as species appears to be rather a conglomerate of subpopulations that have been selected by environmental pressures. The extent to which this phenomenon can be generalized to eucaryotic phytoplankton remains to be seen [*Gallagher et al.*, 1984].

4.4. Response of Coccolithophorid Populations to Changing Climate: An Evolutionary Perspective

[45] Our future projections show that the largest coccolithophorid populations of the world oceans, the North Atlantic, could potentially suffer a major decrease in areal bloom. According to these predictions, approximately 20% of the negative $\Delta N/\Delta t$ values (areas of decreasing nitrate) associated with coccolithophorids pixels observed in our study appear positive in the predicted scenario for the North Atlantic (Figure 9) while these changes are negligible in the North Pacific and in the Southern Ocean. While a drawdown of nutrients is also expected in future climate scenarios, the projected alterations in the nitrate cycling in the North Atlantic are a consequence of changes in deep winter mixing that appear to affect the projected onset of coccolithophorid blooms.

[46] It has been suggested that the progressive increase in atmospheric CO_2 concentrations predicted for the next few decades may decrease the production of calcium carbonate in the surface ocean [*Riebesell et al.*, 2000], and thus this response could potentially act as a negative feedback on atmospheric CO_2 levels. In the equilibrium $CO_2 + H_2O + CaCO_3 \leftrightarrow 2HCO_3^- + Ca^{2+}$, an increase in CO_2 concentration leads to calcium carbonate dissolution, whereas a decrease in CO_2 levels achieves the reverse. While photosynthetic carbon fixation decreases the partial pressure of CO_2 as dissolved inorganic carbon is being utilized, conditions favoring surface calcification by coccolithophorid blooms contribute to the increase of dissolved CO_2. Biologically mediated calcification in upper ocean layers results in Ca oversaturation compared to deep layers, and thus Ca is often precipitated and redissolved several times before it reaches the sediment [*Stumm and Morgan*, 1981]. By the middle of the 21st century, the concentration of CO_{2atm} is predicted to be double that of preindustrial levels [*Houghton*, 1996]. The carbonate ion concentration in seawater controls the rate of precipitation and dissolution of calcium carbonate in the oceans. The relative abundance of the components of the carbonate system (CO_2, H_2CO_3, HCO_3^-, and CO_3^{2-}) depends upon pH, dissolved inorganic carbon, and the total alkalinity. Under modern ocean water conditions (pH 8.0–8.2), $[HCO_3^-]$:$[CO_3^{2-}]$: $[CO_2]$ is approximately 200:10:2. A predicted future pH decrease of 0.35 units caused by the predicted increase in pCO_2 will result in a 30% increase in CO_3^{2-}, and a corresponding 50% increase in dissolved CO_2, that will directly affect marine biota, and will likely change processes of biogenic $CaCO_3$ formation and sedimentation and the elemental composition of primary produced organic and inorganic matter. A future increase in the CO_2:HCO_3^- ratio will diminish the evolutionary advantages of CO_2-concentrating mechanisms present in some phytoplankton taxa including coccolithophorids and diatoms [*Nimer et al.*, 1997; *Iglesias-Rodríguez and Merrett*, 1997] and will reduce the calcium carbonate saturation state of the surface ocean,

$$\Omega = [Ca^{2+}][CO_3^{2-}]/K_{sp},$$

where K_{sp} is the solubility product, largely regulated by pressure [*Byrne and Laurie*, 1999]. Ω is mainly determined by the concentration of CO_3^{2-} because Ca^{2+} is approximately conservative in seawater [*Millero*, 1996]. At pH 7.8, the concentration of CO_3^{2-}would decreases by 30% from modern ocean pH conditions and consequently, it would decrease calcite saturation by an equal percentage. The global production of $CaCO_3$ is $\sim$0.6 Gt C yr^{-1} [*Milliman*, 1993] and represents up to 3% of the global marine carbon fixation [*Berger*, 1976; *Longhurst et al.*, 1995]. In the modern ocean, coccolithophorids alter the $C_{organic}$:$C_{carbonate}$ or "rain ratio" and increase surface pCO_2 during calcification, producing one molecule of CO_2 for each molecule of $CaCO_3$ fixed. Globally, the rain ratio from the surface ocean is roughly 4:1 [*Broecker and Peng*, 1982] and is an important factor in determining the fate of the CO_2 in seawater. This ratio is largely controlled by the dominant taxon fixing carbon such that a shift in the phytoplankton community structure from one functional group to another (e.g., from calcifiers to silicifiers) would affect the capacity of the biological pump in the control of surface pCO_2. For example, during a bloom of coccolithophorids, photosynthesis:calcification and the rain ratio can approach 1:1, and the effect of such high calcification rates has been found to change the air-sea gradient of CO_2 [*Robertson et al.*, 1994]. Considering that coccolithophorid blooms are responsible for up to 80% of surface ocean calcification [*Fabry*, 1989; *Deuser and Ross*, 1989], the 50% predicted decrease in potential surface coccolithophorid bloom areal extent may potentially lead to a significant increase in the POC:PIC ratio. In half a century, under the worse predictions of the Intergovernmental Panel on Climate Change, an increase in dissolved CO_2 and a decrease in the concentration of CO_3^{2-}will result in an increase in calcium carbonate dissolution. Additionally, a potential shift in the phytoplankton community favoring noncalcifying phytoplankters, as a result of projected changes in the mixing dynamics in areas responsible for more than half of the total

annual coccolithophorid bloom areas, will have a major impact on the capacity of the ocean as a reservoir of carbonate. A decrease in calcification is a short-term negative feedback in the global carbon cycle.

[47] **Acknowledgments.** The authors wish to thank Oscar Schofield for his valuable comments and Robert Berk for his helpful discussions. We also thank John Green for providing strains of *Emiliania huxleyi*. This research was supported by the National Aeronautic and Space Administration through the Synthesis and Modeling Program of the U.S. Joint Global Ocean Flux Studies (SMP) under grant NAG5-6982 (to P. G. F.), and the National Science Foundation Biocomplexity Research Program under grant OCE-0084032 (to P. G. F.). The molecular analysis of AFLP was funded by the Natural Environment Research Council under fellowship GT5/99/MS/14 (to M. D. I.-R.). C. W. B. was supported by funding from the NOAA Ocean Remote Sensing Program.

References

Balch, W. M., and K. Kilpatrick, Coccolith production and detachment by *Emiliania huxleyi* (Prymnesiophyceae), *J. Phycol.*, *29*, 566–575, 1993.

Balch, W. M., P. M. Holligan, S. G. Ackleson, and K. J. Voss, Biological and optical properties of mesoscale coccolithophorid blooms in the Gulf of Maine, *Limnol. Oceanogr.*, *36*, 629–643, 1991.

Balch, W. M., P. M. Holligan, and K. A. Kilpatrick, Calcification, photosynthesis and growth of the bloom-forming coccolithophore, *Emiliania huxleyi*, *Cont. Shelf Res.*, *12*, 1353–1374, 1992.

Barker, G. L. A., J. C. Green, P. K. Hayes, and L. L. Medlin, Preliminary results using the RAPD analysis to screen bloom populations of *Emiliania-huxleyi* (Haptophyta), *Sarsia*, *79*, 301–306, 1994.

Berger, W. H., Biogenous deep-sea sediments: production, preservation and interpretation, in *Treatise on Chemical Oceanography*, vol. 5, edited by J. P. Riley and R. Chester, pp. 265–388, Academic, San Diego, Calif., 1976.

Berthon, J. F., and A. Morel, Validation of a spectral light-photosynthesis model and use of the model in conjunction with remotely sensed pigment observations, *Limnol. Oceanogr.*, *37*, 781–796, 1992.

Blackburn, S. I., and G. Cresswell, A coccolithophorid bloom in Jervis Bay, Australia, *Aust. J. Mar. Freshwater Res.*, *44*, 785–786, 1993.

Blackmon, M., et al., The Community Climate System Model, *Bull. Am. Meteorol. Soc.*, *82*, 2357–2376, 2001.

Boville, B. A., and P. R. Gent, The NCAR Climate System Model, version one, *J. Clim.*, *11*, 1115–1130, 1998.

Bown, P. R., and J. R. Young, Mesozoic calcareous nannoplankton classification, *J. Nannoplankton Res.*, *19*, 21–36, 1997.

Broecker, W., and T. H. Peng, *Tracers in the Sea*, Lamont-Doherty Geol. Obs., Columbia Univ., ELDEGEO Press, New York, 1982.

Brown, C. W., Spatial and temporal variability of *Emiliania huxleyi* blooms in SeaWiFS imagery, *Eos Trans. AGU*, *80*(49) Suppl., 153, 1999.

Brown, C. W., and J. A. Yoder, Coccolithophorid blooms in the global ocean, *J. Geophys. Res.*, *99*, 7467–7482, 1994.

Byrne, R. H., and S. H. Laurie, Influence of pressure on chemical equilibria in aqueous systems with particular reference to seawater, *Pure Appl. Chem.*, *71*, 871–890, 1999.

Conkright, M., et al., World Ocean Database 1998, *Natl. Oceanogr. Data Cent. Internal Rep. 14*, 1998.

Denman, K. L., and M. A. Peña, A coupled 1-D biological/physical model of the northeast subarctic Pacific Ocean with iron limitation, *Deep Sea Res., Part II*, *46*, 2877–2908, 1999.

Deuser, W. G., and E. H. Ross, Seasonally abundant planktonic-foraminifera of the Sargasso Sea: Succession, deep-water fluxes, isotopic compositions, and paleoceanographic implications, *J. Foraminiferal Res.*, *19*, 268–293, 1989.

Egge, J. K., and D. L. Aksnes, Silicate as regulating nutrient in phytoplankton competition, *Mar. Ecol. Prog. Ser.*, *83*, 281–289, 1992.

Eppley, R. W., J. N. Rogers, and J. J. McCarthy, Half saturation constant for uptake of nitrate and ammonium by marine phytoplankton, *Limnol. Oceanogr.*, *14*, 912–920, 1969.

Eynaud, F., J. Giradeaux, J.-J. Pichon, and C. J. Pudsey, Sea-surface distribution of coccolithophorid, diatoms, silicoflagellates and dinoflagellates in the South Atlantic Ocean during the late austral summer 1995, *Deep Sea Res., Part I*, *46*, 451–482, 1999.

Fabry, V. J., Aragonite production by pteropod mollusks in the subantarctic Pacific, *Deep Sea Res.*, *36*, 1735–1751, 1989.

Falkowski, P. G., and J. A. Raven (Eds.), *Aquatic Photosynthesis*, Blackwell Sci., Malden, Mass., 1997.

Falkowski, P. G., R. T. Barber, and V. Smetacek, Biogeochemical controls and feedbacks on ocean primary production, *Science*, *281*, 200–206, 1998.

Findlay, C. S., and J. Giraudeau, Extant calcareous nannoplankton in the Australian Sector of the Southern Ocean (austral summers 1994 and 1995), *Mar. Micropaleontol.*, *40*, 417–439, 2000.

Fisher, N. S., and S. Honjo, Intraspecific differences in temperature and salinity responses in the coccolithophorid *Emiliania huxleyi*, *Biol. Oceanogr.*, *6*, 355–361, 1989.

Gallagher, J. C., A. M. Wood, and R. S. Alberte, Ecotypic differentiation in the marine diatom Skeletonema costatum: Influence of light intensity on the photosynthetic apparatus, *Mar. Biol.*, *82*, 121–134, 1984.

Garcia-Soto, C., E. Fernandez, R. D. Pingree, and D. S Harbour, Evolution and structure of a shelf coccolithophorid bloom in the Western English Channel, *J. Plankton Res.*, *17*, 2011–2036, 1995.

Gordon, H. R., and M. Wang, Retrieval of water-leaving radiance and aerosol optical thickness over the oceans with SeaWiFS: A preliminary algorithm, *Appl. Opt.*, *33*, 443–452, 1994.

Grime, J. P., *Plant Strategies and Vegetation Processes*, John Wiley, New York, 1979.

Gruber, N., and J. L. Sarmiento, Global patterns of marine nitrogen fixation and denitrification, *Global Biogeochem. Cycles*, *11*, 235–266, 1997.

Hallegraeff, G. M., Coccolithophorids (calcareous nanoplankton) from Australian waters, *Bot. Mar.*, *27*, 229–247, 1984.

Hay, B. J., M. A. Arthur, W. E. Dean, E. D. Neff, and S. Honjo, Sediment deposition in the late Holocene abyssal Black Sea with climatic and chronological implications, *Deep Sea Res.*, *38*, 1211–1235, 1991.

Heimann, M., and E. Maier-Reimer, On the relations between the oceanic uptake of CO_2 and its carbon isotopes, *Global Biogeochem. Cycles*, *10*, 89–110, 1996.

Henrich, R., Diagenetic environments of authigenic carbonates and opal-Ct crystallization in lower Miocene to upper Oligocene deposits of the Norwegian Sea (ODP Site 643, Leg 104), in *Proceedings of the Ocean Drilling Program*, edited by O. Eldholm, J. Thiede, and E. Taylor, *Sci. Result, 104*, pp. 233–248, Ocean Drill. Program, College Station, Tex., 1989.

Hentschel, E., Die biologische Methoden und das biologische Beobachtungsmaterial der Meteor-Expedition, *Wiss. Ergeb. Atl. Exped. Meteorol.*, *10*, 1–274, 1932.

Hiramatsu, C., and P. De Deckker, Distribution of calcareous nannoplankton near the subtropical convergence, south of Tasmania, Australia, *Mar. Freshwater Res.*, *47*, 707–713, 1996.

Holligan, P. M., M. Viollier, D. S. Harbour, P. Camus, and M. Champagne-Philippe, Satellite and ship studies of coccolithophorid production along a continental shelf edge, *Nature*, *304*, 339–342, 1983.

Holligan, P. M., et al., A biogeochemical study of the coccolithophorid, *Emiliania huxleyi*, in the North Atlantic, *Global Biogeochem. Cycles*, *7*, 879–900, 1993.

Honjo, S., The rain of ocean particles and Earth's carbon cycle, *Oceanus*, *40*, 4–8, 1997.

Houghton, R. A., Converting terrestrial ecosystems from sources to sinks of carbon, *Ambio*, *25*, 267–272, 1996.

Humborg, C., V. Ittekkot, A. Cociasu, and B. V. Bodungen, Effect of Danube River dam on Black Sea biogeochemistry and ecosystem structure, *Nature*, *386*, 385–388, 1997.

Iglesias-Rodríguez, M. D., and M. J. Merrett, Dissolved inorganic carbon utilization and the development of extracellular carbonic anhydrase by the marine diatom *Phaeodactylum tricornutum*, *New Phytol.*, *135*, 163–168, 1997.

Joos, F., and M. Bruno, Long-term variability of the terrestrial and oceanic carbon sinks and the budgets of the carbon isotopes C^{13} and C^{14}, *Global Biogeochem. Cycles*, *12*, 277–295, 1998.

Jordan, R. W., and J. C. Green, A checklist of the extant haptophyta of the world, *J. Mar. Biol. Assoc. U.K.*, *74*, 149–174, 1994.

Ketchum, B. H., The absorption of phosphate and nitrate by illuminated cultures of *Nitzschia closterium*, *Am. J. Bot.*, *26*, 399–407, 1939.

Kinkel, H., J. Young, H. Stoll, P. Ziveri, M. Geissen, I. Probert, and K. H. Baumann, Size matters: The influence of coccolith size and growth rate on paleobarometry and climates, paper presented at 8th International Conference, Nannoplankton Assoc., Bremen, Germany, 2000.

Levitus, S., Climatological Atlas of the World Ocean, *Prof. Pap. 13*, 173 pp., NOAA/ERL Geophys. Fluid Dyn. Lab., Princeton, N.J., 1982.

Lipps, J. H., Fossil Prokaryotes and Protists, Blackwell Sci., Malden, Mass., 1993.

Longhurst, A., S. Sathyendranath, T. Platt, and C. Caverhill, An estimate of global primary production in the ocean from satellite radiometer data, *J. Plankton Res.*, *17*, 1245–1271, 1995.

Malin, G., S. M. Turner, and P. S. Liss, Sulfur: The plankton climate connection, *J. Phycol.*, *28*, 590–597, 1992.

McClain, C. R., M. L. Cleave, G. C. Feldman, W. W. Gregg, S. Hooker, and N. Kuring, Science quality SeaWiFS data for global biosphere research, *Sea Technol.*, September 10–16, 1998.

McIntyre, A., and A. W. H. Bé, *Coccolithus neohelis* sp. N., a coccolith fossil type in contemporary seas, *Deep Sea Res.*, *14*, 369–371, 1967.

Medlin, L. K., G. L. A. Barker, L. Campbell, J. C. Green, P. K. Hayes, D. Marie, S. Wrieden, and D. Vaulot, Genetic characterisation of *Emiliania huxleyi* (Haptophyta), *J. Mar. Syst.*, *9*, 13–31, 1996.

Mihnea, P. E., Major shifts in the phytoplankton community (1980–1994) in the Romanian Black Sea, *Oceanol. Acta*, *20*, 119–129, 1997.

Millero, F. K., *Chemical Oceanography*, CRC Press, Boca Raton, Fla., 1996.

Milliman, J. D., Production and accumulation of calcium carbonate in the ocean: Budget of a nonsteady state, *Global Biogeochem. Cycles*, *7*, 927–957, 1993.

Moore, J. K., S. C. Doney, J. A. Kleypas, D. M. Glover, and I. Y. Fung, An intermediate complexity marine ecosystem model for the global domain, *Deep Sea Res., Part II*, *49*, 403–462, 2001a.

Moore, J. K., S. C. Doney, J. A. Kleypas, D. M. Glover, and I. Y. Fung, Iron cycling and nutrient limitation patterns in surface waters of the World Ocean, *Deep Sea Res, Part II*, *49*, 463–508, 2001b.

Najjar, R. G., and R. F. Keeling, Analysis of the mean annual cycle of the dissolved oxygen anomaly in the World Ocean, *J. Mar. Res.*, *55*, 117–151, 1997.

Nimer, N. A., M. D. Iglesias-Rodríguez, and M. J. Merrett, Bicarbonate utilization by marine phytoplankton species, *J. Phycol.*, *33*, 625–631, 1997.

Paasche, E., S. Brubak, S. Skattbø, J. R. Young, and J. C. Green, Growth and calcification in the coccolithophorid *Emiliania huxleyi* (Haptophyceae) at low salinities, *Phycologia*, *35*, 394–403, 1996.

Pondaven, P., O. Ragueneau, P. Treguer, A. Hauvespre, L. Dezileau, and J. L. Reyss, Resolving the "opal paradox" in the Southern Ocean, *Nature*, *405*, 168–172, 2000.

Quay, P., Carbon sink: The role of oceans, *Geotimes*, *37*, 16–18, 1992.

Raven, J. A., The vacuole: A cost-benefit analysis, *Adv. Bot. Res.*, *25*, 59–86, 1997.

Reynolds, R. W., A real-time global sea surface temperature analysis, *J. Clim.*, *11*, 75–86, 1988.

Reynolds, R. W., and D. C. Marsico, An improved real-time global sea surface temperature analysis, *J. Clim.*, *6*, 114–119, 1993.

Riebesell, U., I. Zondervan, B. Rost, P. D. Tortell, R. E. Zeebe, and F. M. M. Morel, Reduced calcification of marine plankton in response to increased atmospheric CO_2, *Nature*, *407*, 364–367, 2000.

Riegman, R., W. Stolte, A. A. M. Noordeloos, and D. Slezak, Nutrient uptake, and alkaline phosphate (EC 3:1:3:1) activity of *Emiliania huxleyi* (Prymnesiophyceae) during growth under N and P limitation in continuous cultures, *J. Phycol.*, *36*, 87–96, 2000.

Robertson, J. E., C. Robinson, D. R. Turner, P. Holligan, A. J. Watson, P. Boyd, E. Fernandez, and M. Finch, The impact of a coccolithophorid bloom on oceanic carbon uptake in the northeast Atlantic during summer 1991, *Deep Sea Res., Part II*, *41*, 297–314, 1994.

Sarmiento, J. L., J. Dunne, A. Gnanadesikan, R. M. Key, K. Matsumoto, and R. Slater, A new estimate of the $CaCO_3$ to organic carbon export ratio, *Global Biogeochem. Cycles*, *16*, doi:10.1029/2002GB001919, in press, 2002.

Steinke, M., G. Malin, S. D. Archer, P. H. Burkill, and P. S. Liss, Enzymatic production of dimethylsulfide during a coccolithophorid bloom in the North Atlantic, paper presented at American Society of Limnology and Oceanography Aquatic Sciences Meeting, Santa Fe, N.M., 1999.

Stumm, W., and J. J. Morgan, *Aquatic Chemistry: An Introduction Emphasizing Chemical Equilibra In Natural Waters*, John Wiley, New York, 1981.

Thomsen, H. A., K. R. Buck, S. L. Coale, D. L. Garrison, and M. M. Gowing, Nanoplanktonic coccolithophorids (prymnesiophyceae, Haptophyceae) from the Wedell Sea, Antarctica, *Nord. J. Bot.*, *8*, 419–436, 1988.

Trenberth, K. E., Recent observed interdecadal climate changes in the Northern Hemisphere, *Bull. Am. Meteorol. Soc.*, *71*, 988–993, 1990.

Vance, T. C., et al., Aquamarine waters recorded for first time in Eastern Bering Sea, *Eos Trans. AGU*, *79*(10), 121, 1998.

Vos, P., et al., AFLP: A new technique for DNA-fingerprinting, *Nucleic Acids Res.*, *23*, 4407–4414, 1995.

Watabe, N., and K. M. Wilbur, Effects of temperature in growth, calcification and coccolith form in *Coccolithus huxleyi* (Coccolithineae), *Limnol. Oceanogr.*, *11*, 567–575, 1966.

Westbroek, P., P. R. Youn, and K. Linschooten, Coccolith production (biomineralization) in the marine alga *Emiliania huxleyi*, *J. Protozool.*, *36*, 368–373, 1989.

Westbroek, P., et al., A model system approach to biological climate forcing: The example of *Emiliania huxleyi*, *Global Planet. Change*, *8*, 27–46, 1993.

Winter, A., M. Elbrächter, and G. Krause, Subtropical coccolithophorids in the Weddell Sea, *Deep Sea Res., Part I*, *46*, 439–449, 1999.

Wolfe, G. V., E. B. Sherr, and B. F. Sherr, Release and consumption of DMSP from *Emiliania huxleyi* during grazing by *Oxyrrhis Marina*, *Mar. Ecol. Prog. Ser.*, *111*, 111–119, 1994.

Wood, A. M., and T. Leatham, The species concept in phytoplankton ecology, *J. Phycol.*, *28*, 723–729, 1992.

Young, J. R., The functions of coccoliths, in, *Coccolithophorids*, edited by A. Winter and W. G. Siesser, pp. 63–82, Cambridge Univ. Press, New York, 1994.

Young, J. R., and P. Westbroek, Genotypic variation in the coccolithophorid species *Emiliania-huxleyi*, *Mar. Micropaleontol.*, *18*, 5–23, 1991.

C. W. Brown, Office of Research and Applications, National Oceanographic and Atmospheric Administration, 5200 Auth Road, Camp Springs, MD 20746-4304, USA. (christopher.w.brown@noaa.gov)

S. C. Doney and J. Kleypas, National Center for Atmospheric Research, Climate and Global Dynamics, P.O. Box 3000, Boulder, CO 80307-3000, USA. (doney@ucar.edu; kleypas@ucar.edu)

P. G. Falkowski, M. D. Iglesias-Rodríguez, D. Kolber, and Z. Kolber, Environmental Biophysics and Molecular Ecology Program, Institute of Marine and Coastal Sciences, Rutgers University, 71 Dudley Road, New Brunswick, NJ 08901, USA. (falko@imcs.rutgers.edu; iglesias@imcs.rutgers.edu; dkolber@imcs.rutgers.edu; zkolber@imcs.rutgers.edu)

P. K. Hayes, School of Biological Sciences, University of Bristol, Woodland Road, Bristol BS8 1UG, England, U.K. (paul.hayes@bristol.ac.uk)